Simple models of non-Gaussian statistics for a turbulently advected passive scalar

Mark Holzer and Alain Pumir*
Laboratory of Atomic and Solid State Physics, Cornell University, Ithaca, New York 14853-2501
(Received 26 May 1992)

We study the probability distribution of a passive scalar undergoing turbulent mixing in the presence of a mean scalar gradient. Kerstein's model, which describes the turbulent mixing process as a collection of instantaneous local rearrangements of the scalar, is argued to be a plausible approximation when the size of the system is much larger than the velocity correlation length, and after the description has been coarse grained over a correlation volume. In the physical range of parameters, we find numerically that the fluctuations of the scalar θ are close to exponentially distributed when a linear mean scalar gradient is imposed. The phenomenological mean-field-like theory of Pumir, Shraiman, and Siggia [Phys. Rev. Lett. **66**, 2984 (1991)] is derived heuristically beginning with the Kerstein model. This theory predicts strictly exponential tails for the probability distribution of the scalar fluctuations $P(\theta)$, i.e., $P(\theta)\sim\exp(|\theta|)$. We also consider a simplified version of the Kerstein model which is analytically fully tractable and gives qualitatively similar results numerically. Under conditions of spatial homogeneity and imposed linear mean scalar gradient, this simplified model and the full Kerstein model are described by the same mean-field theory. However, for the simplified model, the large-$|\theta|$ asymptotic behavior of $P(\theta)$ is Poisson-like, i.e., $P(\theta)\sim\exp[-|\theta|\ln|\theta/(\text{const})|]$.

PACS number(s): 02.50.−r, 05.40.+j, 47.27.Qb

I. INTRODUCTION

Randomness is an obvious feature of turbulent flows [1]. For this reason, statistical concepts must play an important role in the understanding of their properties. One of the simplest questions to ask in this respect concerns the nature of the probability distributions of various fluctuating quantities, such as velocity or its derivatives, the local rate of dissipation, or the concentration of a passive scalar, the latter being the focus of this paper. Gaussian distributions are ubiquitous as a consequence of the central limit theorem. They can also be found in turbulent flows. For example, velocity fluctuations in grid turbulence are known to be Gaussian [2,3], and Tavoularis and Corrsin [4] showed that the probability density function (PDF) of a passive scalar can also be Gaussian under certain conditions.

However, many fluctuating quantities characterizing turbulent flows are very non-Gaussian. Unlike Gaussian PDF's, non-Gaussian PDF's can reflect interesting physical mechanisms and not merely the law of large numbers. Experimentally, a variety of quantities have been demonstrated to be non-Gaussian. It was clearly shown by Van Atta and Chen [5] that the PDF of velocity differences in atmospheric flows is strongly non-Gaussian. More recent experimental data show in great detail that longitudinal velocity differences $\Delta v_l(r)\equiv[\mathbf{v}(\mathbf{x}+\mathbf{r})-\mathbf{v}(\mathbf{x})]\cdot\hat{\mathbf{r}}$ cross over from an exponential distribution (which decays more slowly than a Gaussian) when r is small, to a Gaussian distribution when r increases beyond a coherence length [6,7]. In the context of turbulent Rayleigh-Bénard convection, it has been shown by Castaing *et al.* [8] and Sano, Wu, and Libchaber [9] that temperature in the center of the experimental cell also has a very non-Gaussian PDF with exponential tails. Recently, direct numerical simulations of turbulent flows [10,11] have confirmed the non-Gaussian character of the distribution of velocity derivatives, while confirming the velocity to be (one-point) Gaussian.

The extant experimental and numerical data suggest that the existence of PDF's with exponential tails is a prevalent phenomenon in turbulence. However, the origin of exponential tails of the PDF of gradients must be very different from the origin of exponential tails for temperature fluctuations. Velocity differences are mainly sensitive to the small-scale structure of turbulence. By contrast, the distribution of temperature fluctuations in a convection experiment has more to do with the spatial organization of the flow. Kraichnan [12] made plausible that the deviation from Gaussian behavior of velocity derivatives can result from the combined influence of nonlinear stretching and viscous diffusion. Various elaborations of his ideas have been proposed recently [13]. Castaing, Gagne, and Hopfinger [14] used alternative approaches, based on cascade ideas.

In this paper, we consider the problem of a passively advected scalar, which is described by the equation

$$\partial_t\Theta+\mathbf{v}\cdot\nabla\Theta=\kappa\nabla^2\Theta\ , \tag{1}$$

where κ is the molecular diffusivity, $\mathbf{v}$ is the turbulent velocity field, and ∂_t denotes a partial derivative with respect to time t. Depending on the particular experimental situation, the scalar, Θ, could be temperature or density of a passive contaminant such as ink. By Θ being *passive*, we mean that the dynamics of the velocity *does not couple to* Θ. Thus Eq. (1) is truly linear in Θ.

Although the passive scalar problem has a long history [15,16], Eq. (1) remains difficult to solve directly—in fact very few interesting solutions have been found to date (see, e.g., Ref. [17]). Part of the problem is, of course,

that the dynamics of the velocity field itself is far from well understood. Because the PDF of a passive scalar reflects the spatial organization of the flow, it is crucial that any approximation of the velocity field reflects the key features of the flow structure.

The striking exponential tails observed in the actively convected system of the experiments of Libchaber and co-workers [8,9] have recently led Pumir, Shraiman, and Siggia [18] to consider the simpler problem of a passive scalar, Eq. (1), in the case where the scalar has a mean gradient. A simple phenomenological mean-field-like theory is constructed which predicts exponential tails for the scalar PDF. In spite of the heuristic nature of the derivation, this prediction has recently found some experimental support. Gollub *et al.* [19] found a PDF with exponential tails for a passive scalar in a stirred system, while Jayesh and Warhaft [20] observed exponential tails in the scalar PDF for grid turbulence in a wind tunnel. In both cases the passive scalar was temperature with an imposed linear mean gradient. For Gollub's experiments, velocity itself was likely strongly non-Gaussian. In Jayesh and Warhaft's experiment the velocity was measured to be (one-point) Gaussian and, in the absence of a mean scalar gradient, the scalar PDF was found to be slightly sub-Gaussian. Non-Gaussian (more slowly decaying than Gaussian) transient scalar PDF's were also found by Métais and Lesieur [21] in a direct numerical simulation of a passive scalar field in three-dimensional Navier-Stokes turbulence. Finally, let us mention that in the case of a stably stratified fluid, the temperature fluctuations have been found, both experimentally [22] and numerically [21], to be almost perfectly Gaussian. The role of buoyancy as a restoring force makes the physics of the stratified fluid very different from that of the convection experiments. The theory developed in this paper must be modified to take the effects of stable stratification into account.

Motivated by the prevalence of non-Gaussian PDF's in recent experiments and also by the apparent success of Ref. [18], we consider here a number of models for a randomly advected scalar in the spirit of the simple lattice models recently introduced by Kerstein [23]. We argue that it is reasonable to approximate the turbulent flow by a random superposition of eddies, of typical size ξ_v (the correlation length or "integral scale"), which is assumed to be much smaller than the size of the system, L. Since one expects that the details of small-scale turbulence are not going to be very important to understand the properties of the passive scalar PDF, we imagine coarse graining the system to the mesoscopic scale ξ_v. The coarse graining renormalizes the diffusivity κ to an effective, much larger, eddy diffusivity κ_e. Consistency of the various physical assumptions leads to a relation between the dimensional parameters that define the model. We will find that Kerstein's "linear-eddy" model [23] (to be called the Kerstein model here) reproduces some of the key properties of a turbulently advected passive scalar when applied to a coarse-grained description of the flow.

The remainder of this paper is structured as follows. Our derivation of the Kerstein model for the passive scalar problem is given in Sec. II. In Sec. III we discuss the numerical implementation of the Kerstein model and present simulation results for one and two dimensions. Deviations from Gaussian behavior, strongly suggestive of exponential tails, are found in the physical range of parameters of the model. PDF's are more Gaussian for another range of parameters. The transition from Gaussian to non-Gaussian is smooth. In an effort to understand better our numerical results, we consider some analytically tractable simplifications of the Kerstein model. In Sec. IV we give a heuristic derivation of the mean-field-like theory of Ref. [18] beginning with the Kerstein model. It is an easy exercise to derive an evolution equation for the PDF of Θ when either only advection or only diffusion acts. The hard and not formally justified step consists of treating the interplay between advection and diffusion by simply adding the two effects. In the theory, the Fourier transform of the PDF has a finite strip of analyticity predicting strictly exponential tails. Our evidence that this theory is a correct "mean-field" description of the Kerstein model comes from comparing the analytical solutions of the former with the numerical solutions of the latter. We also study the mean-field theory for the case of fixed boundary conditions and, separately, for the case of large-scale advection which is superimposed on the meso-scale turbulence. In Sec. V we consider a simplified version of the one-dimensional Kerstein model. Under the conditions of spatial homogeneity and imposed linear mean gradient, the model leads to qualitatively similar results numerically and the mean-field theory approach of the preceding section cannot distinguish between this simplified model and the full Kerstein model. However, the simplified model is completely solvable and we show that the Fourier transform of the PDF is an entire function. The asymptotic behavior of the corresponding PDF of the scalar fluctuations, θ, is a Poisson-like distribution, i.e., $P(\theta) \sim \exp[-|\theta|\ln|\theta/(\text{const})|]$. We summarize and conclude in Sec. VI.

II. THE KERSTEIN MODEL OF TURBULENT MIXING

Rather than attacking the full advective diffusion equation (1) directly, we introduce in this section a simplified, discrete model of turbulent mixing. Although our discrete model is essentially the linear-eddy model of Kerstein [23], we regard it here from a conceptually different point of view. In particular, we do not pay much attention to the small-scale motion of the turbulent flow, and focus, instead, on a coarse-grained description at (what will here be) a mesoscopic length scale, the correlation length, or integral scale, of the flow, ξ_v.

We make the following assumptions.

(i) The energy-containing eddies of the velocity field have a typical size ξ_v much smaller than the size of the system, L. This assumption is very natural in a variety of experimental situations. For example, in grid-turbulence experiments, ξ_v would be of the order of the grid size, typically much smaller than the width of the channel or wind tunnel.

(ii) The variance of the scalar is determined from fluctuations at the integral scale, ξ_v, as is the case for the

variance of the velocity field (in contrast to the variance of scalar derivatives, $\nabla\Theta$, which are determined by the small-scale structure of the flow).

(iii) The velocity field is implicitly assumed to be incompressible, i.e., assumed to satisfy $\nabla\cdot\mathbf{v}=0$.

The nonlinear interactions of hydrodynamics (vortex stretching in three dimensions) generate structures in a self-similar way at smaller and smaller scales down to some viscous dissipation cutoff. Instead of dealing with the resulting wide range of length scales, we imagine here "integrating out" the small scales to get a coarse-grained description of the flow at the integral scale, or correlation length ξ_v. This coarse graining renormalizes the molecular transport coefficients. Since the motion of the fluid at scales smaller than ξ_v is largely disorganized and random, its main effect is to enhance transport properties so that the renormalized quantities are much larger than the "bare" ones [24].

We will not literally carry out the renormalization procedure here. Instead, the renormalized quantities are estimated on dimensional grounds. Velocity fluctuations at a scale smaller than ξ_v can be taken into account by an effective eddy diffusivity κ_e for the scalar, and an effective eddy viscosity ν_e for the velocity field. Let τ_e be the characteristic time scale of eddies of size ξ_v (e.g., the eddy turnover time). We then have $\nu_e\sim\kappa_e\sim\xi_v^2/\tau_e$ so that the resulting turbulent Prandtl number, ν_e/κ_e, is of order unity.

With this coarse-grained picture in mind, consider first the effect of an isolated eddy on the scalar field, Θ. The eddy is characterized by a size ξ_v and a lifetime $\tau_e\sim\xi_v^2/\nu_e$. Let the eddy be centered on the position x_0. Kinematically, the velocity of the eddy rotates the fluid, and, therefore, the passive scalar around x_0. On average, the scalar (over a region of size ξ_v^d) is rotated by about 2π before the eddy disappears. Since the effective Prandtl number is of order unity, the eddy diffuses over a length of order ξ_v during this rotation. The problem of the action of a single eddy of size ξ_v and typical velocity $v\sim\xi_v/\tau_e$ on a passive scalar field with a diffusivity $\kappa_e\sim\xi_v^2/\tau_e$ does not have an analytic solution. However, numerical calculations [25] support our assertion that such an eddy partially rotates the concentration field as described.

Once the small-scale motion of the flow has been integrated out, one is left with a simplified description of the flow as a random superposition of eddies of size ξ_v and characteristic time τ_e. The fluctuations of Θ are driven by this flow and diffuse with an eddy diffusivity $\kappa_e\sim\xi_v^2/\tau_e$.

The difficulty of the passive scalar problem lies in the interplay between advection and diffusion. For our purposes, it suffices to model this process. Consider a one-dimensional situation. The effect of an eddy is to interchange the concentration to the right of x_0 with the concentration to the left of x_0 (see Fig. 1). During this interchange the scalar diffuses. Forgetting about the details of the exact dynamics, the final result is qualitatively the same as that obtained from the succession of the following two operations.

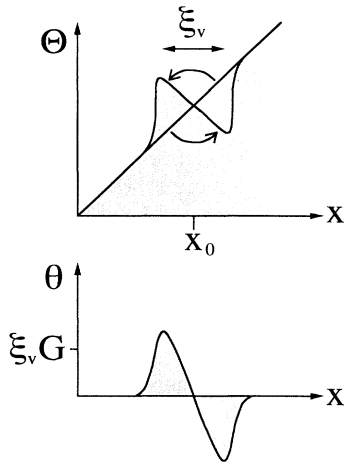

FIG. 1. The action of an eddy of size ξ_v centered at x_0 on the scalar field Θ as modeled by the Kerstein model. The eddy "flips" the scalar to the right of x_0 with the scalar to the left of x_0. When Θ has a mean gradient G, as shown, such a flip produces adjacent blobs of opposite sign and amplitude $\xi_v G$ in the fluctuations $\theta=\Theta-\langle\Theta\rangle$. These flips are performed instantaneously at a random set of space-time locations. Between flips, the scalar diffuses with an eddy diffusivity κ_e which tends to smooth the blobs out.

(1) Move the scalar instantaneously from the right of x_0 to the left of x_0, and vice versa, i.e., *flip* the concentration field (over a region of size ξ_v) around x_0.

(2) Diffuse for a time of order τ_e, with the effective diffusion constant $\kappa_e\sim\xi_v^2/\tau_e$.

Since coarse graining led us to consider the flow as a random superposition of eddies, we arrive at the equation

$$(\partial_t-\kappa_e\nabla^2)\Theta=\text{flip term}\ , \tag{2}$$

where the flip term instantaneously interchanges the scalar to the right of x_0 for $x\in\sim(x_0,x_0+\xi_v/2)$, with the scalar to the left of x_0 for $x\in\sim(x_0-\xi_v/2,x_0)$, at a random set of space-time locations $\{(x_0,t_0)\}$. An important constraint in this model is that the flip term conserves all the moments of the scalar, $\int d\mathbf{x}\,\Theta^n$, as does the advection term $\mathbf{v}\cdot\nabla$ in the original equation for the scalar, Eq. (1). There are a number of ways this can be done; see Sec. III for details. As long as this constraint was satisfied, our numerical results were fairly insensitive to the details of the implementation of the flip term.

We will consider primarily a system homogeneous in space and statistically stationary in time. The space-time locations of the centers of the eddies are therefore chosen to be uniformly distributed. The dimensional parameters of the model are the size of the system, L, the integral length scale ξ_v, the effective diffusivity κ_e, and the space-time density of the flips $\rho\equiv(L^d\tau)^{-1}$, where τ is the average time between flips and d is the spatial dimension. With these parameters two important time scales can be constructed. First, as we have seen before, the charac-

teristic time scale of the eddies is given by $\tau_e=\xi_v^2/\kappa_e$. The time τ_f, defined as the average time that separates two flips affecting the same region of space, is given by $\tau_f=(\rho\xi_v^d)^{-1}$. Assumptions (i) and (ii) above, and their consequence that the flow can be described as a random superposition of eddies, imply that the two times τ_f and τ_e should be of the same order. If $\tau_f \gg \tau_e$, very few eddies (most of the time, none) are active at a given instant of time. Clearly, this does not describe the physics of a turbulent flow. The other limit, $\tau_f \ll \tau_e$, means that many eddies (all of size ξ_v) act on the same region of space within a single eddy-turnover time, which is not physically correct either. Rewriting the condition $\tau_f \sim \tau_e$, one finds that for the model to describe the physics we are interested in, its defining parameters should satisfy the condition

$$K \equiv \frac{\kappa_e}{\xi_v^2}\left[\frac{1}{\rho\xi_v^d}\right] \sim 1 , \tag{3}$$

that is, the dimensionless ratio K should be of order unity.

In the absence of a source term for the scalar fluctuations (given a fluctuating velocity field) the PDF of the scalar fluctuations will eventually relax to a δ function corresponding to a completely mixed state without fluctuations. Although transients of such a relaxation process can be interesting [26–28], we shall be concerned with the case where a source term for the scalar leads to a nontrivial steady-state PDF. To see how such a source term can be introduced in a natural way, write the scalar field as the sum of a fluctuating part, $\theta(\mathbf{x},t)$, and a mean part, $\langle\Theta(\mathbf{x},t)\rangle$, i.e.,

$$\Theta(\mathbf{x},t)=\theta(\mathbf{x},t)+\langle\Theta(\mathbf{x},t)\rangle . \tag{4}$$

Note that if the mean profile $\langle\Theta\rangle$ is linear in $\mathbf{x}$, it is conserved by the advective diffusion equation. Thus, if we take

$$\langle\Theta(\mathbf{x})\rangle=\mathbf{G}\cdot\mathbf{x} , \tag{5}$$

and write Eq. (1) in terms of θ as

$$(\partial_t+\mathbf{v}\cdot\nabla-\kappa_e\nabla^2)\theta(\mathbf{x},t)=-\mathbf{v}\cdot\mathbf{G} , \tag{6}$$

the linear mean gradient is seen to act as a spatially homogeneous source of fluctuations, provided $\mathbf{v}$ is homogeneous.

Some comments about the choice of a linear mean gradient are in order. A nonlinear mean profile at $t=0$ will relax to a linear one in the absence of additional forcing. On the other hand, if some large-scale motion (on scales much larger than the integral scale) is imposed on the system, it is possible that the steady state has a nonlinear mean gradient so that $\mathbf{G}$ on the right-hand side of (6) has $\mathbf{x}$ dependence. (Such is the case, for example, in the experiments of Libchaber and co-workers [8,9], where large-scale motion across the cell persists.) This loss of spatial homogeneity will clearly influence the statistics of the fluctuations and can itself be sufficient to lead to non-Gaussian behavior [29]. We concentrate here mainly on a linear gradient so that we do not have to disentangle the more complicated effects of spatial inhomogeneity from the intrinsic effects of the turbulent mixing.

In the following, it will be useful to have in mind an intuitive picture of the steady state, as produced by the linear mean gradient, in terms of the Kerstein model. Consider one dimension and suppose $\Theta(t=0)=xG$. The action of an eddy on the scalar field, modeled as a flip in Θ of size ξ_v, moves a blob of higher mean concentration into a region of lower mean concentration and vice versa, as depicted in Fig. 1. In the fluctuations, θ, this produces adjacent blobs of opposite sign and amplitude of order $\xi_v G$. The amplitude of the blobs decreases in the subsequent diffusion which spreads the blobs out. A statistically stationary state is achieved when the rate at which flips produce blobs balances the rate at which they are destroyed by the smoothing action of diffusion. In the physical regime of the model, $K\sim 1$, diffusion has on average just enough time to smooth out a given blob before it is created again. Hence we expect the root-mean-square (rms) value of θ, σ, to be of order $\xi_v G$ in this regime. The unphysical regime, $K\gg 1$, corresponds to the case of rare eddies, or equivalently, to strong diffusion between flips. We expect the corresponding variance of the PDF to be very narrow. The other unphysical extreme, $K\ll 1$, corresponds to the case of many eddies acting on the same region of space within a single eddy-turnover time. This is modeled here by weak diffusion between successive flips so that a given region is visited randomly by many "up blobs" and "down blobs" within one diffusion time τ_e. Thus, at any given x, $\theta(x)$ undergoes a random walk of many steps per τ_e. We expect exact Gaussian behavior and diverging variance in the limit $K\to 0$. For small but finite K the PDF should have a well-defined Gaussian core.

III. NUMERICAL STUDY OF THE KERSTEIN MODEL

We implemented model (2) numerically in one and two dimensions (1D and 2D). Consider first 1D; the generalization to 2D is then straightforward. The system has length L and is discretized into a lattice of N evenly spaced points, labeled by n. We impose a mean gradient and periodic boundary conditions on the fluctuations, i.e., $\theta_n=\theta_{n+N}$. At each of a set of randomly chosen, uniformly distributed times, a single flip acts on a randomly chosen position. The requirement that the times at which a flip occurs be uniformly distributed implies that the time between flips, Δt, is distributed according to the distribution

$$P(\Delta t)=\frac{1}{\tau}\exp(-\Delta t/\tau) , \tag{7}$$

where $\tau=(\rho L^d)^{-1}$ is the average time between successive flips.

Between flips, the system evolves according to the diffusion equation, $(\partial_t-\kappa_e\nabla^2)\theta=0$. This equation is efficiently and accurately integrated for a time t by using fast Fourier transforms (FFT's) to multiply the spatial Fourier modes, θ_k, by $\exp(-\kappa_e t k^2)$. We set $\theta(\mathbf{x},t=0)$ and evolve the system until a statistically stationary state has been reached. Subsequently, the values of θ at the N

points of the lattice are recorded precisely every $\tau_s \sim 5\tau$ and accumulated in a histogram, our numerical approximation to the PDF, $P(\theta)$. This is done sufficiently many times to obtain good statistics down to $P(\theta/\sigma) \sim 10^{-6}$. Error bars on $P(\theta)$ were estimated from the fluctuations between several histograms (typically ten), each computed for a different realization of the space-time distribution of flips.

To complete the numerical implementation of the model, we need to specify precisely how a flip is to be performed. To do this, it is sufficient to specify an area-preserving mapping, $\mathbf{x} \rightarrow \mathbf{x}'$, of the coordinates in the region to be affected by the eddy, onto themselves. The full concentration $\Theta(\mathbf{x},t)$ is then simply carried along by the mapping, i.e., $\Theta'(\mathbf{x}')=\Theta(\mathbf{x})$, or in terms of the fluctuations,

$$\theta'(\mathbf{x}')=\theta(\mathbf{x})+(\mathbf{x}-\mathbf{x}')\cdot\mathbf{G} \ . \tag{8}$$

The area-preserving property of the mapping ensures the conservation of the PDF of the scalar, i.e., of all the moments $\int d\mathbf{x}\,\Theta^n(\mathbf{x})$.

Perhaps the simplest and most literal way to implement a flip in one dimension is to simply reflect the full concentration $\Theta(\mathbf{x},t)$ about the midpoint of the "eddy," x_0. Explicitly,

$$x \rightarrow x'=2x_0-x \ , \tag{9}$$

for $x_0-l \le x \le x_0+l$, where l is the "eddy radius." The minimal lattice representation of (9) (minimal in terms of number of lattice points involved) is to take

$$(\theta_n,\theta_{n+1}) \rightarrow (\theta_{n+1}+aG,\theta_n-aG) \ , \tag{10}$$

where $a \equiv L/N$ is the lattice constant. Multisite implementations follow analogously. If $l=a/2$ as in (10), we can expect some artifacts in $P(\theta)$ due to the very discretized nature of this flip. On the other hand, if l is large, the reflection flip (9) introduces sharp discontinuities at its edge. Although we shall find that these discontinuities have no adverse effect on $P(\theta)$, one may wish to get rid of them, especially if one were interested (like Kerstein) in the spatial spectrum of the fluctuations. One way to accomplish this is to mix the coordinates between x_0-l and x_0+l according to the triplet map T, defined as follows:

$$x \rightarrow x'=\begin{cases} +3[x-(x_0-l)]+x_0-l & \text{if } x_0-l \le x < x_0-l/3 \\ -3[x-(x_0-l/3)]+x_0+l & \text{if } x_0-l/3 \le x < x_0+l/3 \\ +3[x-(x_0+l/3)]+x_0-l & \text{if } x_0+l/3 \le x < x_0+l \ . \end{cases} \tag{11}$$

The map T is not invertible. It stretches the scalar on the three subintervals, $(x_0-l,x_0-l/3)$, $(x_0-l/3,x_0+l/3)$, and $(x_0+l/3,x_0+l)$. This mapping has been used successfully by Kerstein to model all sorts of turbulent mixing processes [23]. As a minimal lattice representation of (11) we take

$$(\theta_n,\theta_{n+1},\theta_{n+2},\theta_{n+3}) \rightarrow (\theta_{n+2}+2aG,\theta_{n+3}+2aG,\theta_n-2aG,\theta_{n+1}-2aG) \ . \tag{12}$$

Again, multisite discrete versions follow in an analogous fashion from the full mapping. A natural choice for ξ_v for all the flips discussed is to take $\xi_v \equiv 2l$. Before discussing the implementation of the Kerstein model in 2D let us look at the numerical results in 1D.

In all our numerical simulations we have adopted units such that $\kappa_e=1$, $G=N/2\pi$, and $L=2\pi$. (In these units, a σ of $\xi_v G$ will have the same numerical value as ξ_v in units of lattice spacings.) We consider first a 32-site system with the simplest possible kind of flip, Eq. (10), and $\xi_v \equiv a$. Figure 2 shows the correlation function $\langle\theta(0)\theta(r)\rangle$ as a function of r for $K=8.300\times10^{-2}$, 1.660, and 16.60. The correlation length for the scalar, ξ_θ, is seen to be about one lattice spacing almost independently of K. Thus, in the presence of a linear mean scalar gradient, $\xi_\theta \sim \xi_v$, as we might have expected. Figures 3(a)–3(c) show the corresponding PDF's. The unphysical case of rapid flip rate, $K=8.300\times10^{-2} \ll 1$, [Fig. 3(a)] is seen to have a well-defined Gaussian core. However, large fluctuations are slightly more probable than in the case of a Gaussian distribution. The PDF changes smoothly as K is increased. In Fig. 3(b), $K=1.660\sim1$

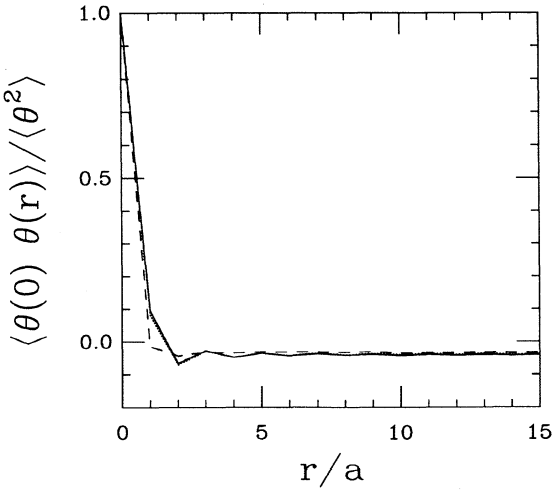

FIG. 2. The correlation function $\langle\theta(0)\theta(r)\rangle/\langle\theta^2\rangle$ vs r/a (a is the lattice spacing) for a 32-site system with the simplest possible reflection flip (1,2)→(2,1), Eq. (10). K was computed with $\xi_v \equiv a$. The three curves are for three different values of K. The solid line is for $K=16.60$, the dotted line for $K=1.660$, and the dashed line for $K=8.300\times10^{-2}$. The figure implies a correlation length for the scalar, ξ_θ, of about one lattice spacing so that $\xi_\theta \sim \xi_v$, virtually independently of K.

and the PDF is seen to be strongly non-Gaussian. The almost straight lines on the semilogarithmic plot for large $|\theta|$ suggest exponential tails. Close to the center, small shoulders have developed. When flips are rare, $K=16.60\gg1$ [Fig. 3(c)], the PDF narrows and shoulders become more pronounced. Note that the shoulders (the points of high curvature) are located at integer multiples of aG which is the amplitude of blobs created by each flip [see Eq. (10)]. In a more realistic system, the amplitude of blobs generated by the eddies would be smoothly distributed and such shoulders would be absent from the PDF. The shoulders are an artifact of discretization and we shall demonstrate below that they disappear if the flip size is distributed smoothly.

Next, we consider a 64-site system with the simplest possible triplet-map flip, Eq. (12), and $\xi_v\equiv3a$. We find that the correlation function again has virtually no K dependence and infer a scalar correlation length $\xi_\theta\sim3a$, so that again $\xi_\theta\sim\xi_v$. Qualitatively, the situation here is the same as it was for the simple two-site flip of the preceding paragraph. Figures 4(a) and 4(b) show the steady-state PDF's in the regimes $K\sim1$ and $K\gg1$, respectively. The main shoulder is seen to be located at $2aG$ as expected from the blob amplitude of the flip, Eq. (12). We attribute the smaller shoulder seen in the rare-flip regime, $K\gg1$, [Fig. 4(b)] at $|\theta|\sim0.6aG$, to the more complicated spatial structure of the flip.

For the reflection flips, Eq. (9), we have also studied the

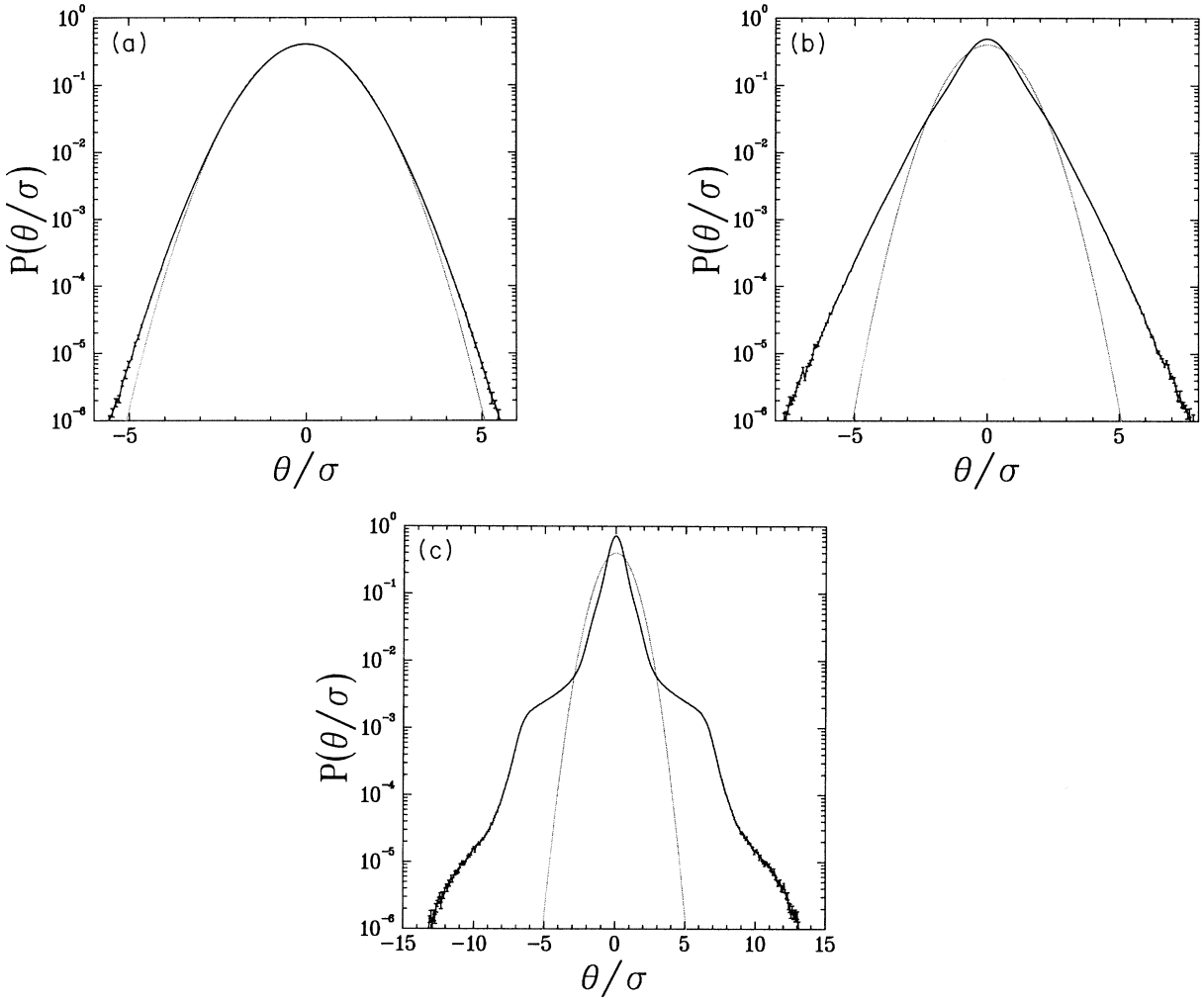

FIG. 3. The PDF of θ for a 32-site system in 1D with the simplest reflection flip $(1,2)\rightarrow(2,1)$, Eq. (10). As a reference, a Gaussian of the same variance is shown (gray line). Each PDF was obtained from ten realizations of the flip distribution. For a given realization, the system was evolved until 5×10^6 flips occurred. K was computed with $\xi_v\equiv a$. (a) $K=8.300\times10^{-2}\ll1$. θ has a rms value σ of 1.906 and a kurtosis of 3.131. The PDF is close to Gaussian with large fluctuations slightly more probable than for a pure Gaussian. (b) $K=1.660\sim1$. θ has a rms value σ of 0.4568 and a kurtosis of 4.552. The PDF is strongly non-Gaussian. The nearly straight lines on this semilogarithmic plot for large $|\theta|$ suggest exponential tails. (c) $K=16.60\gg1$. θ has a rms value σ of 0.1488 and a kurtosis of 15.85. The PDF is strongly non-Gaussian. The shoulders of the PDF occur at approximately integer multiples of aG (at multiples of $|\theta/\sigma|\sim6.7$). The shoulders are a result of the extremely discretized nature of the two-site eddy.

effects of a flip size l which is distributed with the half-Gaussian probability density

$$P(l)=\left[\frac{2}{\pi l_0^2}\right]^{1/2}\exp[-\tfrac{1}{2}(l/l_0)^2],\quad l\geq 0\ . \tag{13}$$

The main motivation for doing this is to mitigate any artifacts due to discretization. Other than a marked suppression of the shoulders of the PDF for $K\geq 1$, we find no qualitative changes from the previous two cases. Figure 5(a) shows the PDF for a 2048-site system with

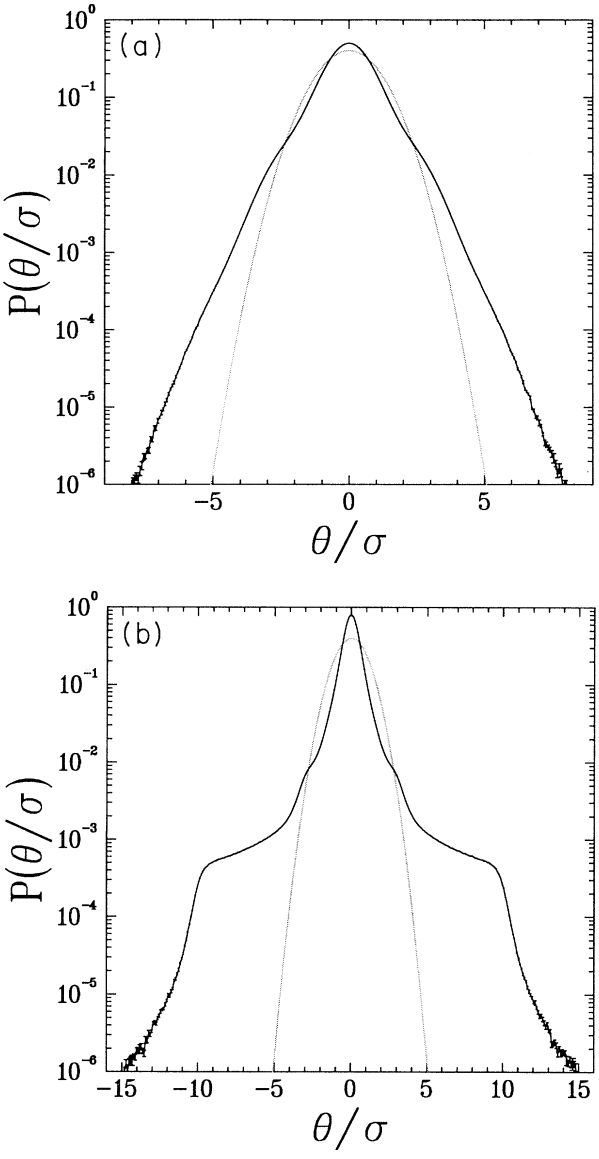

FIG. 4. The PDF of θ for a 64-site system in 1D with the simplest triplet-map flip, Eq. (12). As a reference, a Gaussian of the same variance is shown (gray line). The PDF was obtained from ten realizations of the flip distribution. Each realization was run until 5×10^6 flips occurred. K was computed with $\xi_v\equiv 3a$. (a) $K=0.7378\sim 1$. θ has a rms value σ of 0.6920 and a kurtosis of 4.983. The PDF is strongly non-Gaussian and the nearly straight lines on this semilogarithmic plot for large $|\theta|$ suggest exponential tails. (b) $K=9.837\gg 1$. θ has a rms value σ of 0.2002 and a kurtosis of 28.55. The PDF is strongly non-Gaussian. The pronounced shoulder is located at $2aG$ as expected from the blob amplitude of the flip. We attribute the smaller shoulder at $\sim 0.6aG$ to the more complicated spatial structure of the flip.

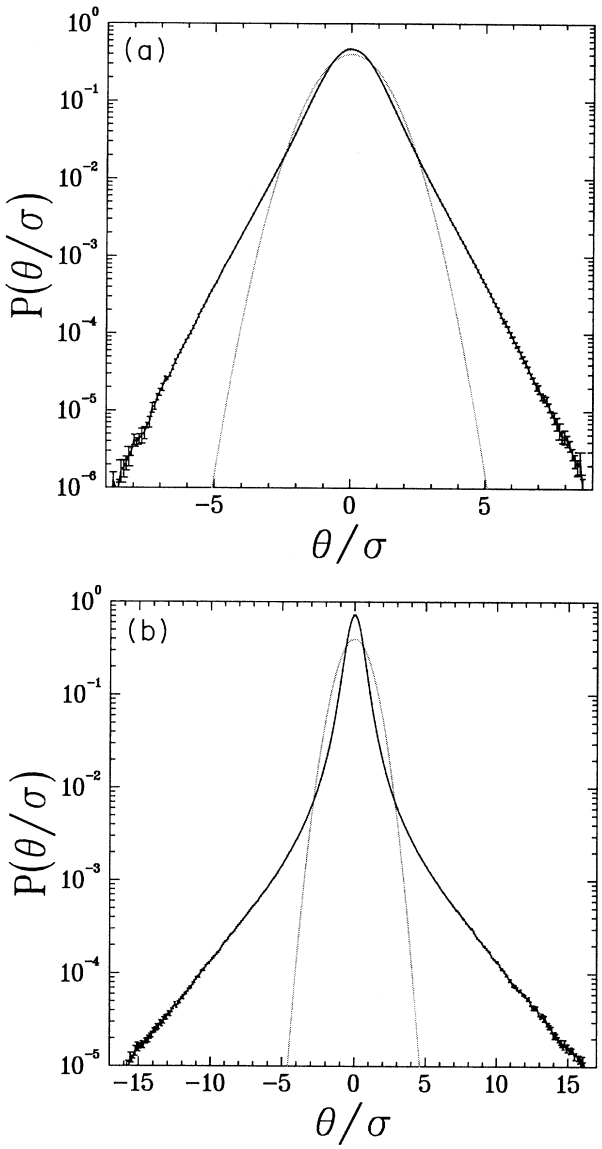

FIG. 5. The PDF of θ for a 2048-site system in 1D and a reflection-map flip, Eq. (9), whose size, l is half-Gaussian distributed with a rms value of $l_0=16a$. As a reference a Gaussian of the same variance is shown (gray line). The PDF was obtained from ten realizations of the flip distribution. Each realization was run until 5×10^4 flips occurred. K was computed with $\xi_v\equiv 2\langle l\rangle=\sqrt{8/\pi}l_0$. (a) $K=0.6536\sim 1$. θ has a rms value σ of 15.82 and a kurtosis of 4.972. The PDF appears to have well-defined exponential tails. Shoulders are barely detectable since the Gaussian-distributed eddy size mitigates any artifacts due to discretization. (b) $K=13.07\gg 1$. θ has a rms value σ of 4.082 and a kurtosis of 30.18. Note the striking absence of any shoulders and the near-exponential tails for $|\theta/\sigma|>\sim 6$.

$l_0 = 16a$ in the regime $K \sim 1$, and Fig. 5(b) shows the PDF for the same system in the rare-flip regime, $K \gg 1$. K was computed with $\xi_v \equiv 2\langle l \rangle = \sqrt{8/\pi} l_0$. A scalar correlation length of $\xi_\theta \simeq 22a \sim \xi_v$ was determined from the scalar correlation functions. Shoulders are barely detectable and their absence is particularly striking in the rare-flip regime, $K \gg 1$, for which Fig. 5(b) suggests exponential tails beyond about six standard deviations. Note that for $K \sim 1$, $\sigma = 15.82$ is of the order of $\xi_v G = 25.53$ as expected [30]. For large $l_0 > 4a$ we find that the variance of the PDF is approximately 2.3 times larger than it would be if (13) were replaced by $\delta(l - l_0)$.

To make sure that the qualitative features of $P(\theta)$ do not depend on dimensionality, we have also implemented the Kerstein model in 2D. The system is taken to be an $L \times L$ square discretized into an $N \times N$ square lattice. Just as in 1D, only one flip acts at a time with the times between flips exponentially [cf. Eq. (7)] distributed. The flip or eddy consists of a rotation by 90° about the center of a square unit cell with a random sense of rotation. The square on which the flip is centered is chosen randomly for each flip. In our simplest version of this flip, only the four sites of the square are involved in the rotation (a "four-site flip"). In a slightly more elaborate version (a "12-site flip"), used to mitigate discreteness effects, the eight nearest neighbors attached to the central unit cell are also rotated (by the same angle in the same sense). Explicitly,

$$\begin{bmatrix} x \\ y \end{bmatrix} \rightarrow \begin{bmatrix} x' \\ y' \end{bmatrix} = s \begin{bmatrix} y - y_0 \\ -x + x_0 \end{bmatrix} + \begin{bmatrix} x_0 \\ y_0 \end{bmatrix}, \tag{14}$$

where $s = \pm 1$, chosen randomly for each flip. The lattice sites involved in this mapping for the two variants of the flip implementation are shown in Fig. 6.

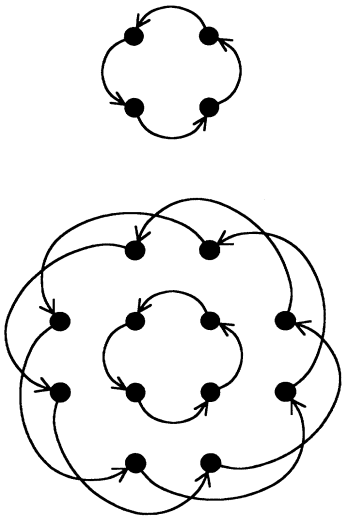

FIG. 6. The sites of a square lattice involved in the flip implementations for 2D. The "four flip" (top) involves the sites of an elementary square of the lattice. The "12 flip" (bottom) involves the sites of a four flip as well as the attached nearest neighbors. The flip itself consists of rotating the scalar on these sites randomly either clockwise or counterclockwise by 90°. A counterclockwise flip is indicated by the arrows.

The main upshot of the simulations in 2D is that the qualitative behavior of the PDF's generated by the Kerstein model does not depend on dimensionality. For the unphysical rapid-flip case, $K \ll 1$, the PDF's are close to Gaussian as expected. For the regimes $K \sim 1$ and $K \gg 1$,

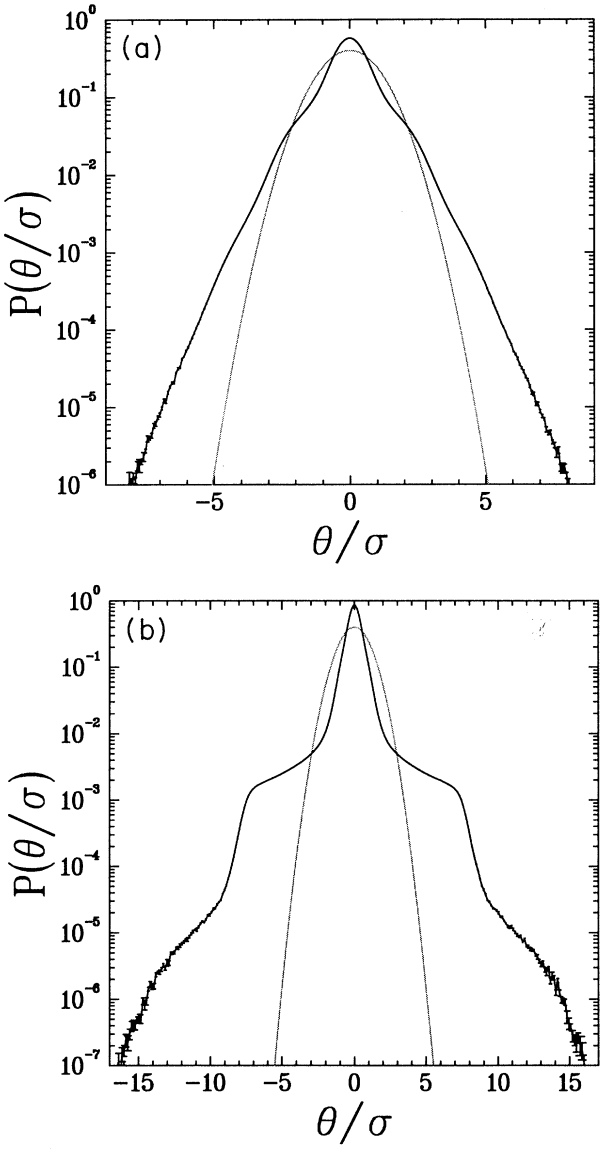

FIG. 7. The PDF of θ for a 32×32-site system in 2D with four-site flips. As a reference, a Gaussian of the same variance is shown (gray line). The PDF's were obtained from ten realizations of the flip distribution. Each realization was run until 2×10^5 flips occurred. K was computed with $\xi_v \equiv a$. (a) $K = 1.328 \sim 1$. θ has a rms value σ of 0.3967 and a kurtosis of 5.318. The PDF displays the expected close-to-exponential tails for large $|\theta|$, (b) $K = 13.28 \gg 1$. θ has a rms value σ of 0.1316 and a kurtosis of 23.16. The PDF is strongly non-Gaussian with shoulders at integer multiples of aG, the blob amplitude of the flip.

the results of the numerical simulations are shown in Figs. 7(a) and 7(b) for the four-site flips and in Figs. 8(a) and 8(b) for the 12-site flips. To determine K, we took $\xi_v \equiv a$ and $\xi_v \equiv 2a$ for the four-site and 12-site flips, respectively. In the rare-flip regime, $K \gg 1$, the four-site flips produce shoulders at integer multiples of aG which is the blob amplitude associated with the flip. For the 12-site flips, the main shoulder is located at $2aG$, and a smaller shoulder develops at aG, as expected from the blob amplitudes associated with the outer and inner sites of the flip, respectively. The PDF's are seen to be qualitatively similar to those obtained in one dimension.

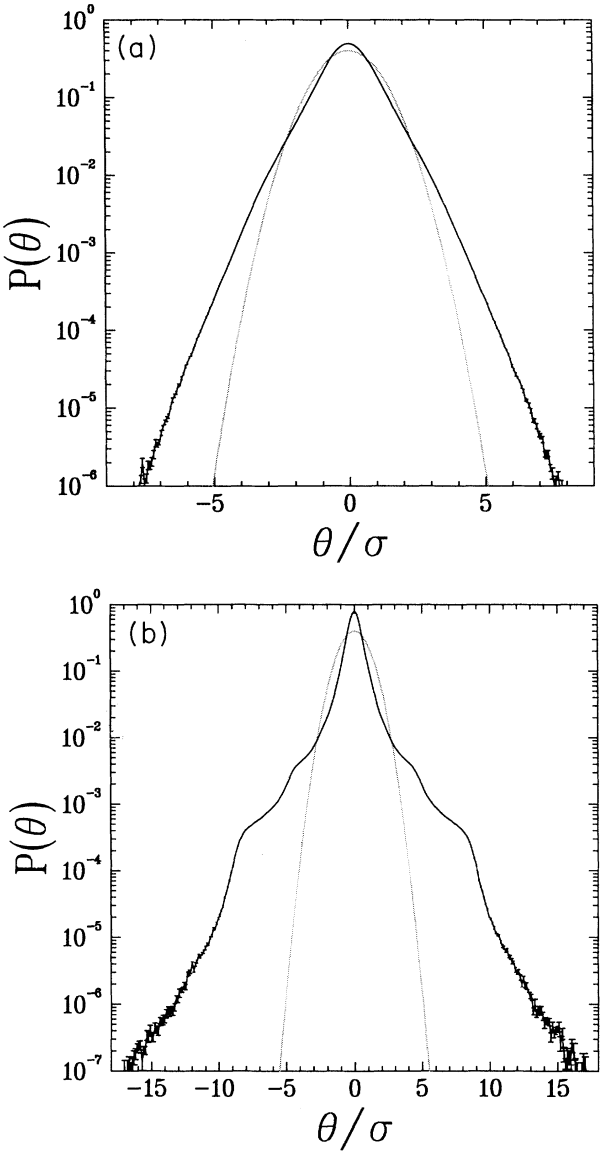

FIG. 8. The PDF of θ for a 32×32-site system in 2D with 12-site flips. As a reference, a Gaussian of the same variance is shown (gray line). The PDF's were obtained from ten realizations of the flip distribution. Each realization was run until 2×10^5 flips occurred. K was computed with $\xi_v \equiv 2a$. (a) $K = 1.660 \sim 1$. θ has a rms value σ of 0.6643 and a kurtosis of 4.678. The PDF displays the expected close-to-exponential tails for large $|\theta|$. Shoulders here are less pronounced than in the corresponding case with four-site flips [Fig. 7(a)] because of the less discretized nature of the 12-site flip. (b) $K = 16.60 \gg 1$. θ has a rms value σ of 0.2308 and a kurtosis of 17.64. The main shoulder is located at $2aG$, and the smaller shoulder at aG, as expected from the blob amplitudes associated with the outer and inner sites of the flip, respectively (see Fig. 6).

IV. MEAN-FIELD THEORY OF THE KERSTEIN MODEL

In this section, we will try to understand better our numerical results. The discussion here is restricted to the one-dimensional case. The main idea is to derive the phenomenological model of Ref. [18] as a mean-field-like description of the Kerstein model, Eq. (2). Our derivation remains at a heuristic level, and involves a very essential, *ad hoc* approximation. We find qualitative agreement between the solutions of the mean-field-like model (and its rapid-flip generalizations for $K \ll 1$) and the numerical solutions of the preceding section.

The two essential ingredients of the Kerstein model (2) are (i) random flips and (ii) diffusion. We will only consider the simplest possible flip, (1,2)→(2,1), Eq. (10). Recall that in this version of the Kerstein model, the correlation length ξ_v is approximately equal to the lattice spacing a, which we will take to be unity here. If we ignore diffusion for the moment, the model is completely solvable. Consider an initial condition without any fluctuations around the mean profile, i.e., $\Theta(x,t=0)=Gx$ and $\theta(x,0)=0$. In the absence of molecular diffusion, a fluid element, advected by the random flips, just carries the scalar along. The flips then induce a random walk in space. The probability that a random flip occurs between t and $t+\Delta t$, and induces a jump from site i to site $i+1$ (or $i-1$) is $p = 1-\exp(-\rho a \Delta t)$. Although we will eventually be interested in $\Delta t \sim (\rho a)^{-1}$, assume for now that $\Delta t \ll (\rho a)^{-1}$. Then, up to corrections of order $(\Delta t)^2$, the equation for the PDF of Θ reads

$$P(\Theta,i,t+\Delta t) = (1-2p)P(\Theta,i,t) + p[P(\Theta,i+1,t)+P(\Theta,i-1,t)] . \quad (15)$$

By taking the Fourier transform of $P(\Theta)$ with respect to Θ, i.e.,

$$\hat{P}_k(i,t) = \int e^{ik\Theta} P(\Theta,i,t)\, d\Theta ,$$
$$P(\Theta,i,t) = \frac{1}{2\pi}\int e^{-ik\Theta}\hat{P}_k(i,t)\, dk , \quad (16)$$

and using the statistical homogeneity of the system, it is easy to solve Eq. (15) exactly. The result is that $P(\Theta,x,t)$ tends to a Gaussian distribution with a variance growing linearly with time. For our purposes here, it is more useful to expand the right-hand side of (15) to obtain, in the continuum limit, the Fokker-Planck equation

$$P(\Theta,x,t+\Delta t) = P(\Theta,x,t) + D\frac{\partial^2}{\partial x^2}P(\Theta,x,t) , \quad (17)$$

where $D \equiv \rho a^2$. Equation (17) makes the connection between random flips and a random walk process obvious:

the flips induce diffusion of the PDF.

The other ingredient of the modified Kerstein model is molecular diffusion. If only diffusion (no flips) is present, $\Theta(x,t)$ is easily obtained from any initial value ($t=0$) as

$$\Theta(x,t)=\int g(x,x',t)\Theta(x',t=0)dx' , \tag{18}$$

where $g(x,x',t)=[1/(4\pi\kappa_e t)^{1/2}]\exp[-(x-x')^2/4\kappa_e t]$ is the Green function of the diffusion equation. Although it is an approximation, let us truncate the sum obtained by discretizing (18) in space (spacing a), and retain only a finite number of terms. When $\tau_e \ll a^2/\kappa_e$, this truncation leads to the standard finite difference representation of the diffusion equation

$$\Theta(i,t)=(1-2\epsilon)\Theta(i,0)+\epsilon[\Theta(i+1,0)+\Theta(i-1,0)] , \tag{19}$$

where $\epsilon=\kappa_e t/a^2$. When t is of the order of the eddy-turnover time, $\tau_e \sim \xi_v^2/\kappa_e$, the truncations we have used,

$$\Theta(i,t)\sim\tfrac{1}{2}[\Theta(i+1,0)+\Theta(i-1,0)] , \tag{20}$$

with $\epsilon=\frac{1}{2}$, or

$$\Theta(i,t)\sim\tfrac{1}{2}\Theta(i,0)+\tfrac{1}{4}[\Theta(i+1,0)+\Theta(i-1,0)] , \tag{21}$$

with $\epsilon=\frac{1}{4}$, although physically sensible, become more questionable mathematically. While neither of them captures exactly the details of the diffusion process, they are both expected to lead to qualitatively correct results. The equation for the time evolution of the PDF can now be obtained from any of Eqs. (19)–(21). While the correlation length of the scalar, ξ_θ, is of the order of $\xi_v \sim 1$, we may consider $\Theta(i+1)$ and $\Theta(i-1)$ to be statistically independent and express $P(\Theta,i,t)$ in terms of one-point functions. Consider, for example, Eq. (20), which then implies that

$$P(\Theta,i,t)=\int P(\Theta',i+1,0)P(2\Theta-\Theta',i-1,0)d\Theta' . \tag{22}$$

Spatial homogeneity allows us to write

$$P(\Theta',i+1,0)P(2\Theta-\Theta',i-1,0) \sim P(\Theta',i,0)P(2\Theta-\Theta',i,0) , \tag{23}$$

so that after Fourier transforming P with respect to Θ, we obtain

$$\hat{P}_k(i,t)=\hat{P}_{k/2}(i,0)^2 . \tag{24}$$

Parallel steps show that (19) leads to

$$\hat{P}_k(i,t)=\hat{P}_{k(1-2\epsilon)}(i,0)\hat{P}_{k\epsilon}(i,0)^2 . \tag{25}$$

Note that Eq. (25) cannot be correct after many iterations, since it explicitly assumes that the correlation length remains small [Eq. (23)], which is not the case in a purely diffusive process. Equation (25) can only be a reasonable approximation for the effect of diffusion if advection acts to keep the correlation length small, as expected from our simulations (see Fig. 2).

To take into account the combined action of flips *and* molecular diffusion requires, even at this level, an additional approximation. We will model the coupling between flips and diffusion by merely adding up the two effects, finally giving

$$\hat{P}_k(x,t+\Delta t)=D\nabla^2\hat{P}_k(x,t)+\hat{P}_{k/2}(x,t)^2 , \tag{26}$$

as obtained from Eq. (24) or

$$\hat{P}_k(x,t+\Delta t)=D\nabla^2\hat{P}_k(x,t)+\hat{P}_{k(1-2\epsilon)}\hat{P}_{k\epsilon}(x,t)^2 , \tag{27}$$

as obtained from Eq. (25) [31]. In these equations we no longer consider Δt small but of order $(\rho a)^{-1}$, with the spatial diffusion term capturing the essential physics of the flips. Equations (26) and (27) describe the time evolution of the PDF in terms of a discrete mapping. Partial differential equations for the PDF are replaced by mappings here as a consequence of coarse graining, which allows us to consider the flow as a random superposition of eddies which act instantaneously at a discrete set of space-time points.

Because the nth moment of $P(\Theta)$ is given by

$$\langle\Theta(x,t)^n\rangle=\left[\left[-i\frac{\partial}{\partial k}\right]^n\hat{P}_k(x,t)\right]_{k=0} , \tag{28}$$

it is easy to check that Eqs. (26) and (27) respect the normalization condition $P_{k=0}(x,t)=1$, and that the average concentration obeys

$$\langle\Theta(x,t+\Delta t)\rangle=\langle\Theta(x,t)\rangle+D\frac{\partial^2}{\partial x^2}\langle\Theta(x,t)\rangle . \tag{29}$$

Since (29) is satisfied, it follows that a linear concentration profile is, indeed, a steady-state solution. Because our modeling of the combined influence of diffusion and advection by adding the Fourier transform of the two effects is completely *ad hoc*, the best evidence we have that Eqs. (26) and (27) are correct is a comparison of their solutions with the numerical solutions of the discrete model obtained in Sec. III.

We now proceed to find the steady-state solutions of Eqs. (26) and (27), when $\langle\Theta\rangle$ is a linear profile, extending from $-\infty$ to $+\infty$. Because of spatial homogeneity, we look for a solution that depends on x through $\langle\Theta\rangle$ only, i.e., for a solution of the form $P(\Theta,x)=P(\Theta-Gx,0)=P(\theta)$, or equivalently of the form

$$\hat{P}_k(x)=\Phi(k)\exp(iGkx) . \tag{30}$$

The normalization condition and the equation $\langle\Theta(x)\rangle=Gx$ impose the constraints $\Phi(0)=1$ and $\partial\Phi(0)/\partial k=0$. Inserting (30) into (26), one obtains

$$\Phi(k)(1+DG^2k^2)=\Phi^2(k/2) , \tag{31}$$

whose solution can be written in terms of an infinite product as

$$\Phi(k)^{-1}=\prod_{n=0}^{\infty}(1+DG^2k^2/2^{2n})^{2^n} . \tag{32}$$

The absolute convergence of the right-hand side of (32) can easily be checked for all finite values of k. The function $\Phi(k)$ is therefore analytic, and has poles for purely imaginary values of k at $k_{\pm n}=\pm i2^n/G\sqrt{D}$. From this

analytic structure it follows that the large-$|\theta|$ behavior of the Fourier transform is given by [32]

$$P(\theta)\simeq\exp\left[-\frac{|\theta|}{G\sqrt{D}}\right],\quad |\theta|\to\infty\ , \tag{33}$$

with a smooth behavior near $\theta=0$. $P(\theta)$ does not have any obvious Gaussian form for small θ. It can be checked directly that the solution (30)–(32) is a stable solution of the mapping defined by Eq. (26).

Although the algebra is lengthier, the steady-state solution of (27) can similarly be found to have the infinite product representation

$$\Phi(k)^{-1}=\prod_{n=0}^{\infty}\prod_{p=0}^{n}[1+DG^2k^2\epsilon^{2p}(1-2\epsilon)^{2(n-p)}]^{2^p\binom{n}{p}}. \tag{34}$$

The absolute convergence of this infinite product can again be checked, thus proving that $\Phi(k)$ is an analytic function. As was the case for Eq. (32), $\Phi(k)$ given by (34) has a countable set of poles at a finite distance from the real axis. The large-$|\theta|$ behavior of the PDF is, therefore, again given by Eq. (33).

We now show that, when ϵ is very small, one recovers a Gaussian distribution near the center (around $\theta=0$). In order to see this property, expand the logarithm of $\Phi(k)$ in powers of k:

$$\ln\Phi(k)=\sum_{q=1}^{\infty}\frac{(-1)^q}{q}D^qG^{2q}k^{2q}\frac{1}{1-[(1-2\epsilon)^{2q}+2\epsilon^{2q}]}\ . \tag{35}$$

The Fourier transform of $\Phi(k)$,

$$P(\theta)=\frac{1}{2\pi}\int e^{-ik\Theta+\ln\Phi(k)}dk\ , \tag{36}$$

can be approximated with the saddle-point method. Provided $|\theta|\ll\sqrt{D}/\epsilon$, one may retain only the first term of the right-hand side of Eq. (35) to find

$$P(\theta)\sim\exp\left[-\frac{\epsilon\theta^2}{DG^2}\right]. \tag{37}$$

The approximation leading to (37) breaks down for $\theta\sim\sqrt{D}/\epsilon$. When $\theta\sim\sqrt{D}/\epsilon$, the value of Eq. (37) matches with that of the asymptotic expression (33), suggesting a crossover from a Gaussian center to the exponential distribution, Eq. (33). A more thorough study of Eq. (36), and a numerical calculation of the Fourier transform of $\Phi(k)$, Eq. (34), confirm this conclusion. To conclude, under conditions of homogeneity and imposed mean scalar gradient, we find qualitative agreement with the numerical solutions of the Kerstein model presented in the preceding section.

It is also relevant experimentally to consider the role of boundary conditions. Typically [19], realistic boundary conditions are a fixed value for the scalar (e.g., temperature) at the sides of the cell. If $\Theta=-\frac{1}{2}$ at $x=0$, and $\Theta=\frac{1}{2}$ at $x=L$, the boundary conditions for the PDF are

$$\begin{aligned}&P(\Theta,x=0)=\delta(\Theta+\tfrac{1}{2})\ ,\\ &P(\Theta,x=L)=\delta(\Theta-\tfrac{1}{2})\ .\end{aligned} \tag{38}$$

In Eq. (26) we will take $L=1$ since L can always be scaled out with the substitution $D\to D'=D/L^2$. The coefficient D' can be thought of as the square of the ratio between the typical size of the eddies, ξ_v, and the size of the system, L. In the steady state, $\langle\Theta(x)\rangle=(x-\frac{1}{2})G$, with $G=1/L=1$ [cf. Eq. (29)].

The solution of Eq. (26), with the boundary conditions (38) cannot be given by (32), since it must involve a singular contribution in order to match with the δ functions at the boundaries. The singular part of the solution can be identified by its large-k behavior. We write the PDF as a sum of singular and regular parts as

$$\hat{P}=\hat{S}+\hat{R}\ , \tag{39}$$

where the regular part, $\hat{R}$, is characterized by

$$\lim_{k\to\infty}\hat{R}_k=0\ , \tag{40}$$

and the singular part, $\hat{S}$, by

$$\lim_{k\to\infty}\hat{S}_k\neq 0\ . \tag{41}$$

To obtain an equation for $\hat{S}_k(x)$, we substitute $\hat{P}_k=\hat{S}_k+\hat{R}_k$ into Eq. (26) and consider the $k\to\infty$ limit. Then, by definition, terms involving only $\hat{R}_k$ will vanish. Cross terms $\hat{R}_{k/2}\hat{S}_{k/2}$ vanish also since the limit of $\hat{S}_k$ at large values of k must be finite if S is to have a meaningful Fourier transform. Thus $\hat{S}_k$ is seen to satisfy

$$\hat{S}_k(x,t+\Delta t)=D\partial_x^2\hat{S}_k(x,t)+\hat{S}_{k/2}^2(x,t)\ , \tag{42}$$

with boundary conditions $\hat{S}_k(x=0)=e^{-ik/2}$ and $\hat{S}_k(x=1)=e^{ik/2}$. In the steady state, (42) may be rewritten in terms of the Green function $g(x|x')$ of the Laplacian as

$$\begin{aligned}\hat{S}_k(x)=&\,xe^{ik/2}+(1-x)e^{-ik/2}\\ &+\int_0^L dx'g(x|x')[\hat{S}_k(x')-\hat{S}_k^2(x')]\ .\end{aligned} \tag{43}$$

Formally solving (43) by iteration shows $\hat{S}_k$ to be comprised of a dense set of δ functions which results from the repeated (spatial) convolution of the δ functions at the boundaries. These δ functions are located at 0 and at $\Theta=\pm p/2^n$, where $n\geq 1$ and $p=1,3,\ldots,2n-1$.

To get some insight into the physics of the singular part of the PDF, we now consider the total weight of the δ functions, $W(x)\equiv\hat{S}_{k=0}(x)$. It follows from (42) that $W(x)$ satisfies the ordinary differential equation [18]

$$D\frac{d^2W(x)}{dx^2}=W(x)-W^2(x)\ , \tag{44}$$

with the boundary conditions $W(0)=W(1)=1$. Any physical solution of (44) must satisfy $0\leq W\leq 1$. Equation (44) has a mechanical analog and describes the motion of a particle of mass D in a potential $V(W)=W^2/2-W^3/3$, x being the "time." The boundary conditions imply that the particle must be in the bottom of the potential well at $x=0$ and 1. A trivial solution of (44) is $W=1$, uniformly; it describes a solution of (26) made up of δ functions only. Other solutions exist provided the half period of

oscillation in the potential well, $\pi/\sqrt{D}$, is larger than unity, i.e., if $D<1/\pi^2$. For $D<1/\pi^2$, this nontrivial solution is the stable solution of the iteration (42). When $D\ll 1/\pi^2$ (a very light particle), the particle spends much of its time near $W=0$ and goes from 1 to 0 in a time of order $\sqrt{D}$. In terms of the scalar, these solutions have the following interpretation. The mathematical transition at ($D=1/\pi^2$) occurs when the size of the system becomes comparable to the size of the eddies. When D is very small (a very large system) the physical solution is equal to the solution (30), with boundary layers of size $\sqrt{D}$ near the walls. In other words, the solution adjusts to its bulk value at a distance of the order of the size of the eddies. When the system size is very small compared to the size of the eddies, a completely unphysical limit, no mixing occurs, and the PDF is made of a set of δ functions.

We have confirmed this picture by numerically solving the equation for the complete PDF (singular plus regular parts), Eq. (26), when the boundary conditions (38) are imposed. The steady state is found by iterating

$$\left[1-D\frac{\partial^2}{\partial x^2}\right]\hat{P}_k^{n+1}(x,t)=[\hat{P}_{k/2}^n(x)]^2\ , \tag{45}$$

where n labels the iteration. A cubic spline interpolation in k was used to compute $\hat{P}_{k/2}$. When $D\ll 1/\pi^2$, the solution in the center of the system ($x=\frac{1}{2}$) can be fit well

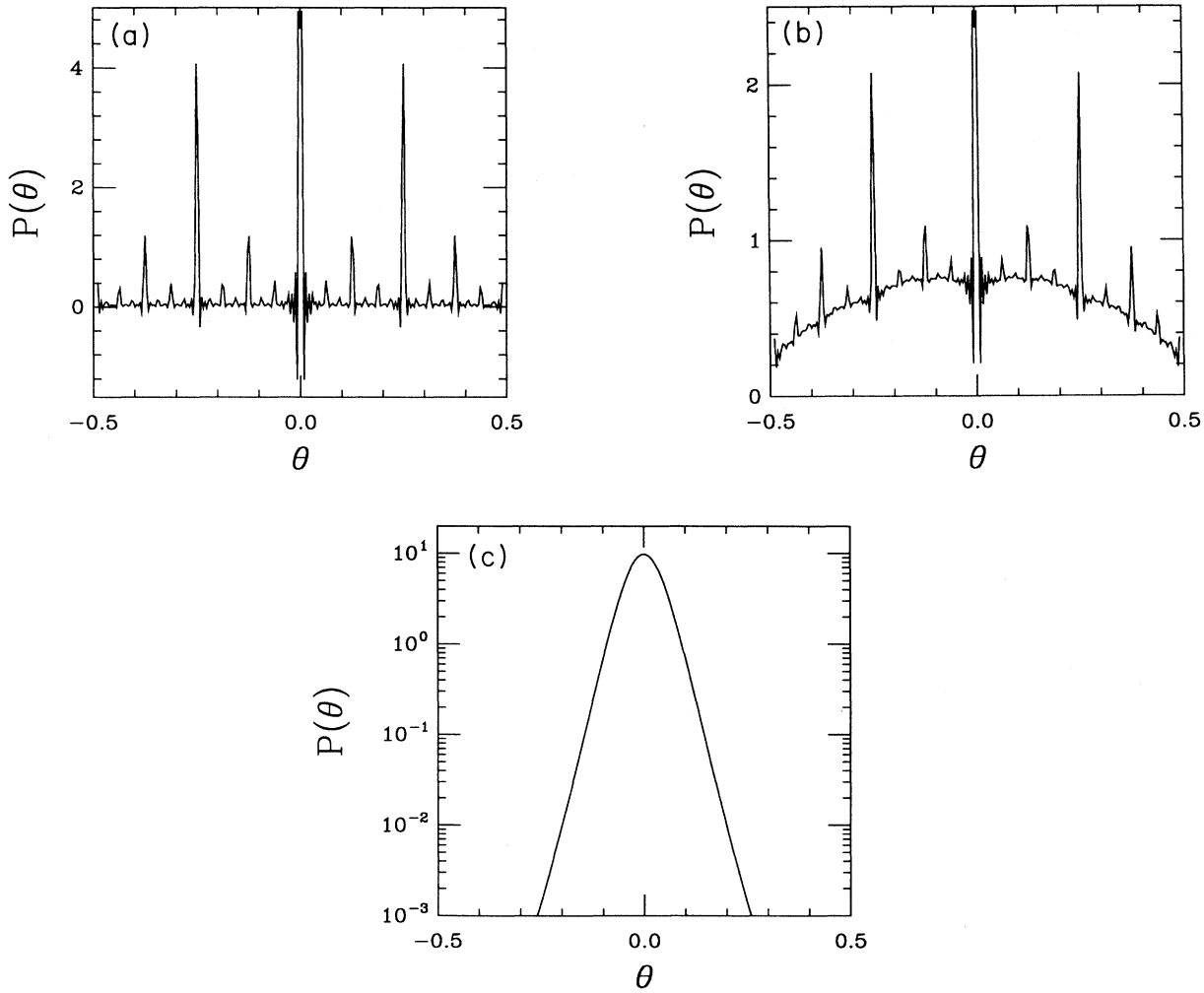

FIG. 9. The solution of the mean-field equation for $P(\Theta)$, Eq. (45), at the center of the system when δ-function boundary conditions are imposed. (At the center of the system, $\langle\Theta\rangle=0$ so that $\Theta=\theta$.) Space was discretized into 201 equally spaced points, and Θ was resolved into 200 wave vectors, k, with a spacing $\Delta k\equiv\pi$. Three very different regimes are shown here. In (a), $D=0.2>1/\pi^2$ and the solution consists of δ functions only [the central peak (height 16.2) has been truncated]. The oscillations (and occasionally negative PDF) close to the peaks are a numerical artifact. In (b), $D=0.05$ and the solution consists of discrete peaks, superposed on a continuous background [again, the central peak (height 6.64) has been truncated]. In (c), $D=5\times10^{-4}$; the peaks are no longer visible and the numerical solution suggests exponential tails.

by the function $\Phi(k)$, Eq. (32). When D gets closer to $1/\pi^2$, the solution in real space near $x=\frac{1}{2}$ shows peaks, superimposed on a continuous background. Figures 9(a)–9(c) show the numerical solution of the mean-field equation (45) with the δ-function boundary conditions (38), for $D=0.2$, 0.05, and 5×10^{-4}, respectively, at the center of the system, $x=\frac{1}{2}$. For $D=0.2$, the solution is seen to be comprised of δ functions, broadened in the figures by our finite numerical resolution. For $D=5\times10^{-4}\ll1/\pi^2$, the peaks are invisible with our numerical resolution and the solution is very close to the bulk solution, Eqs. (32) and (33). Closer to the transition, the solution for $D=0.05$ has both a continuous and a singular part (δ functions). When x approaches the walls (not shown), the peaks of the PDF become asymmetrically weighted toward the appropriate boundary value.

In many real experiments, large-scale flow plays an important role in the mixing process. For example, in turbulent convection experiments, a coherent large-scale eddy is known to persist up to very high Rayleigh number. It is well known [33] that such a recirculating motion tends to expel the gradients from the center, thus dramatically modifying the mean concentration profile in the system. To take into account this large-scale motion, we assume that the flow is a superposition of a large, steady eddy of size L, and many smaller random eddies, of size $\sim\xi_v$, as in Sec. II. The large-scale eddy is modeled by a mapping that first stretches the system by a factor of 3, and then folds it back onto itself (a version of Baker's transformation [34]). More specifically, the mapping

$$x\rightarrow 3x\ , \tag{46}$$

for $0\le x\le L$, is followed by

$$x\rightarrow\begin{cases} x & \text{for } 0\le x\le L \\ 2L-x & \text{for } L\le x\le 2L \\ -2L+x & \text{for } 2L\le x\le 3L\ . \end{cases} \tag{47}$$

This mapping is nothing but the inverse of the triplet map of Sec. II. After one complete mapping, (46) and (47), heat in a small interval $[x,x+\Delta x]$ comes from the three subintervals that have been stretched and folded back onto this interval so that

$$\Theta'(x)\Delta x=\sum_{i=1}^{3}\Theta(x_i)\Delta x_i\ . \tag{48}$$

The sum in (48) may be thought of as extending over the three "preimages" of x involved in the triplet map. Because the stretching here is spatially uniform, $\Delta x_i=\Delta x/3$, giving

$$\Theta'(x)=\tfrac{1}{3}\sum_{i=1}^{3}\Theta(x_i)\ . \tag{49}$$

Under the action of this transformation, the PDF of Θ is transformed according to

$$P(\Theta,x)\rightarrow\int\prod_{i=1}^{3}d\Theta_i P(\Theta_i,x_i)\delta\left[\Theta-\tfrac{1}{3}\sum_{i=1}^{3}\Theta_i\right]\ , \tag{50}$$

or, in terms of the Fourier transform with respect to Θ,

$$\hat{P}_k(x)\rightarrow\prod_{i=1}^{3}\hat{P}_{k/3}(x_i)\ . \tag{51}$$

We are thus led to model the combined action of random advection, large-scale advection, and diffusion by writing [18]

$$\hat{P}_k(x,t+\tau)=\lambda\hat{P}^2_{k/2}+(1-\lambda)\prod_{i=1}^{3}\hat{P}_{k/3}(x_i)+D\frac{\partial^2\hat{P}_k(x,t)}{\partial x^2}\ , \tag{52}$$

where $0\le\lambda\le1$. Equation (52) properly conserves $\int dx\,\Theta(x)$. The equation for the equilibrium mean value of the scalar, $\langle\Theta\rangle$, becomes

$$(1-\lambda)\left[\langle\Theta(x)\rangle-\tfrac{1}{3}\sum_{i=1}^{3}\langle\Theta(x_i)\rangle\right]=D\frac{\partial^2\langle\Theta\rangle}{\partial x^2}\ , \tag{53}$$

which shows that the mean temperature depends only on the ratio $D/(1-\lambda)$.

The steady-state solutions for the PDF of Θ and for $\langle\Theta\rangle$ were found numerically. δ-function boundary conditions were imposed at the walls. As before, the length of the system is set to unity, so that D is proportional to $(\xi_v/L)^2$. Figure 10 shows the computed average profile for $\lambda=0.9$ and $D=0.005$. Figure 11 shows the corresponding PDF at $x=\frac{1}{2}$, the center of the system. The PDF is seen to have clear exponential tails. Away from

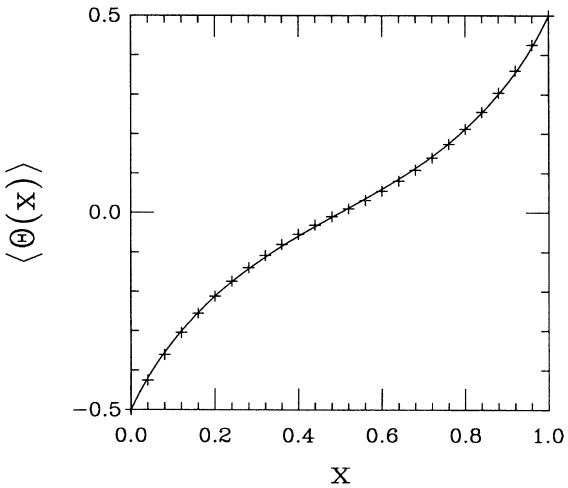

FIG. 10. The mean concentration profile $\langle\Theta(x)\rangle$ in the presence of large-scale flow as modeled in the text. The profile shown is a solution of Eq. (53) with $\lambda=0.9$, $D=5\times10^{-3}$, and δ-function boundary conditions. Space was discretized into 201 equally spaced points, and Θ was resolved into 200 wave vectors, k, with a spacing $\Delta k\equiv\pi$. The crosses indicate a least-squares fit to the empirical form $x'/[1+c(\frac{1}{2}-|x'|)]$, with $x'=x-\frac{1}{2}$ and $c=0.462\sqrt{(1-\lambda)/D}$. We find that $\langle\Theta(x)\rangle$ can be fit well by this approximate form with $c/\sqrt{(1-\lambda)/D}$ of order unity if $D/(1-\lambda)\in\sim(10^{-3},0.1)$. For values of $D/(1-\lambda)<\sim10^{-3}$, $\langle\Theta(x)\rangle$ becomes nonmonotonic.

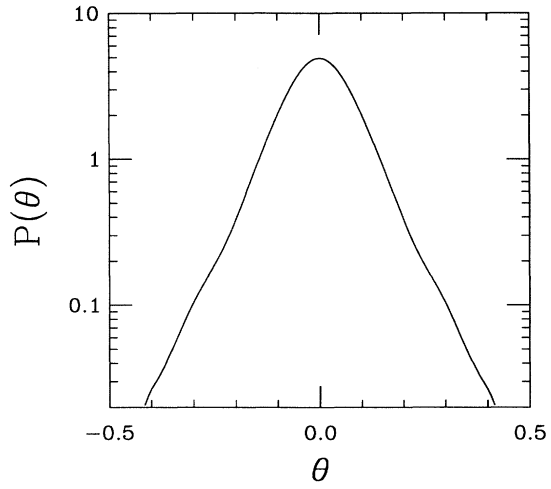

FIG. 11. The solution of the mean-field equation for $P(\Theta)$, Eq. (52), at the center of the system when large-scale flow and δ-function boundary conditions are imposed. (At the center of the system, $\langle\Theta\rangle=0$ so that $\Theta=\theta$.) Space was discretized into 201 equally spaced points, and Θ was resolved into 200 wave vectors, k, with a spacing $\Delta k\equiv\pi$. Corresponding to Fig. 10, $D=5\times10^{-3}$ and $\lambda=0.9$.

the center of the system, the PDF has a more complicated structure.

V. ANALYTICAL SOLUTION FOR A SIMPLIFIED VARIANT OF THE KERSTEIN MODEL

In this section we take a look at a simplified variant of the Kerstein model. Our motivation for doing this is to get some additional insight into the detailed mechanisms responsible for non-Gaussian PDF's and to obtain a model which is directly amenable to analytical treatment without having to resort to a mean-field-like description.

The Kerstein flip has two ingredients: (i) the interchange of the concentration field between adjacent regions and (ii) (in the presence of a linear mean gradient) the generation of adjacent blobs of opposite sign [cf. Fig. 1]. Since, for a given diffusivity, it is clearly the second ingredient which is responsible for a nontrivial steady state, we ask how the steady-state PDF's are affected if we omit the first ingredient. To that end consider the "flip"

$$(\theta_n,\theta_{n+1})\rightarrow(\theta_n+aG,\theta_{n+1}-aG)\ , \tag{54}$$

which we may regard as the simplest reflection flip, Eq. (10), without the spatial interchange of the scalar.

If we were to derive a mean-field-like theory for this model following the methodology of the preceding section, we would replace Eq. (15) for the evolution of the PDF in the absence of molecular diffusion by

$$\begin{aligned}P(\Theta,x,t+\Delta t)&=(1-2p)P(\Theta,x,t)\\&\quad+p[P(\Theta+aG,x,t)+P(\Theta-aG,x,t)]\\&\simeq P(\Theta,x,t)+p(aG)^2\frac{\partial^2}{\partial\Theta^2}P(\Theta,x,t)\ .\end{aligned} \tag{55}$$

This is just Eq. (15) with the flip-induced spatial diffusion replaced by flip-induced diffusion in Θ. However, under conditions of spatial homogeneity and imposed linear mean gradient, the flip-induced diffusion term contributes a term $D(Gk)^2P_k(x,t)$ to the evolution equation for $P_k(x,t)$, with $D\equiv pa^2$, for both flip models. After adding the effect of molecular diffusion, the resulting mean-field theory for model (54) is indistinguishable from that for the full Kerstein model.

Figures 12(a) and 12(b) show the PDF's obtained when this model is numerically implemented with the identical parameters of Figs. 3(b) and 3(c), respectively. For $K\sim1$ [Fig. 12(a)], the model gives close-to-exponential tails. The PDF's of the simplified model are seen to have no qualitative differences from the corresponding PDF's of the full model. In fact, the PDF's are virtually identical. This suggests that the important feature of the flip in the Kerstein model is the fact that up and down blobs are spatially correlated. Indeed, we find that if they are uncorrelated, i.e., if the "flip" consists of $(\theta_n,\theta_{n+r})\rightarrow(\theta_n+aG,\theta_{n+r}-aG)$, with r a randomly chosen site, the PDF for the same parameters as in Fig. 12(a) is nearly perfectly Gaussian. (For larger values of τ, non-Gaussian features appear again even in the uncorrelated case.) We note that the important spatial correlations between up and down blobs, which are equally important for the full Kerstein model, are completely ignored by the mean-field theory.

The model (54) has the advantage of allowing us to immediately write down an analytical expression for the PDF, $P(\theta)$. Consider a space-time strip of dimensions $L\times T$, containing $M=\rho LT$ flips which are uniformly distributed. We will take the limit $M\rightarrow\infty$ (fixed ρ and L) shortly. Space is discrete with $2N$ sites, lattice constant $a=L/2N$, and time is continuous, as in the simulations. With $\theta_n(t=-T)=0$, we can immediately write down $\theta_{n=0}(t=0)$ in terms of the Green function $g_{n,m}(t)$ as

$$\begin{aligned}\theta_{n=0}[t,\{m,t\}]&=\sum_{i=1}^{M}[g_{0,m_i}(t-t_i)-g_{0,m_i+1}(t-t_i)]\\&\equiv\sum_{i=1}^{M}u_{m_i}(t_i)\ ,\end{aligned} \tag{56}$$

where the $\{m_i,t_i\}$ are the space-time locations of the flips. The Green function $g_{n,m}(t-t')$ obeys

$$(\partial_t-\kappa_e\Delta_n)g_{n,m}(t-t')=aG\delta_{n,m}\delta(t-t')\ , \tag{57}$$

where Δ_n is the Laplacian suitably defined for the lattice. For our numerical simulations we have chosen

$$\Delta_n=\frac{1}{a^2}\partial_n^2\ . \tag{58}$$

For this choice, the Green function becomes

$$g_{n,m}(t)=\frac{aG}{2N}\sum_{j=-N}^{N-1} e^{-i(n-m)ak_j}e^{-k_j^2\kappa_e t}H(t)\ , \qquad (59)$$

where $k_j\equiv 2\pi j/L$ and $H(t)$ is the Heaviside step function. In order to compare analytical expressions quantitatively with the simulations, we carefully specify the sum over reciprocal lattice vectors to correspond to the FFT algorithm. This is necessary since with the choice (58), there is no periodicity in the reciprocal space [35].

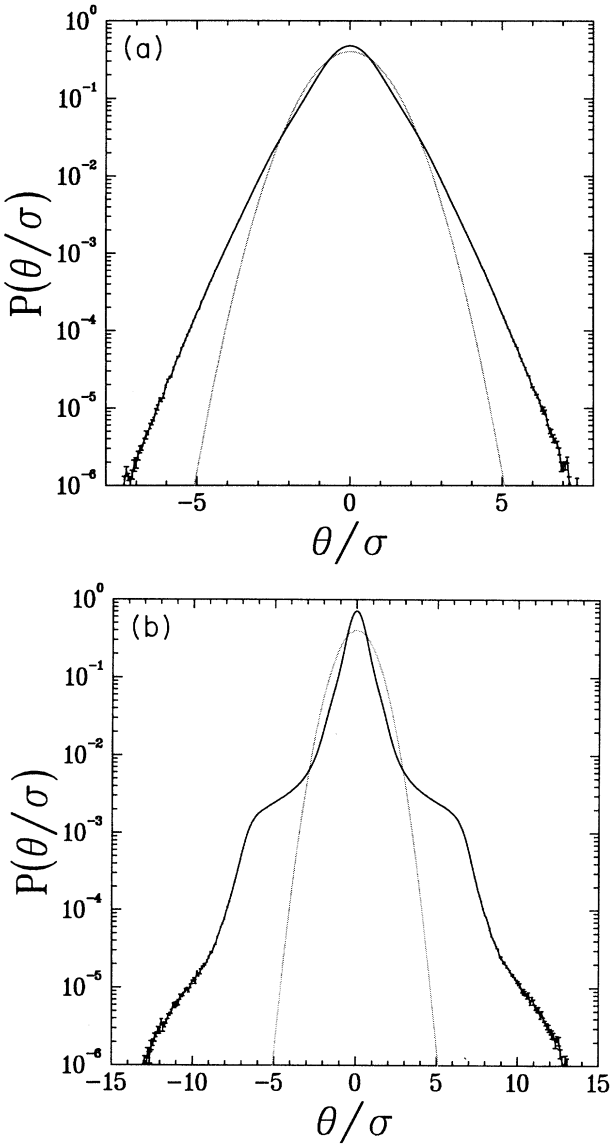

FIG. 12. The PDF's for the simplified variant of the Kerstein model, $(1,2)\rightarrow(1+aG,2-aG)$, implemented on a 32-site lattice in 1D. As a reference, a Gaussian of the same variance is shown (gray line). Each PDF was obtained from ten realizations of the flip distribution. For a given realization, the system was evolved until 5×10^6 flips occurred. Parts (a) and (b) of this figure have the same parameters as Figs. 3(b) and 3(c) for the full Kerstein model, respectively. K was computed with $\xi_v\equiv a$. (a) $K=1.660\sim1$. θ has a rms value σ of 0.472 86 and a kurtosis of 4.255. The PDF is strongly non-Gaussian and equally as suggestive of exponential tails as Fig. 3(b). Indeed, the PDF is virtually identical to that of Fig. 3(b). (b) $K=16.60\gg1$. θ has a rms value σ of 0.149 57 and a kurtosis of 15.52. The PDF is strongly non-Gaussian with shoulders at approximately integer multiples of aG. The PDF is again virtually identical to the corresponding PDF of Fig. 3(c).

Since the flips are uniformly distributed over the space-time strip, we have the following expression for $P(\theta)$:

$$P(\theta)=\left[\prod_{i=1}^{M}\frac{\rho a}{M}\sum_{m_i=-N}^{N-1}\int_0^T dt_i\right]\delta(\theta-\theta[0,\{m,t\}])\ . \qquad (60)$$

Substituting the solution for $\theta[t=0,\{m,t\}]$, Eq. (56), we obtain

$$P(\theta)=\int\frac{dq}{2\pi}e^{iq\theta}\left[\frac{\rho a}{M}\sum_{m=-N}^{N-1}\int_0^T dt\, e^{-iqu_m(t)}\right]^M . \qquad (61)$$

Separating out the $q=0$ contribution to the term in the large parentheses of (61), which is equal to unity, we obtain on taking the limit $M\rightarrow\infty$ that

$$P(\theta_{n=0})=\int_{-\infty}^{\infty}\frac{dq}{2\pi}e^{iq\theta}\hat{P}(q)\ , \qquad (62)$$

where

$$\hat{P}(q)=\exp\left[-\rho a\sum_{m=-N}^{N-1}\int_0^\infty dt\{1-\cos[qu_m(t)]\}\right] . \qquad (63)$$

From $\hat{P}(q)$, moments are easily obtained [cf. Eq. (28)]. In particular, the variance is given by

$$\langle\theta^2\rangle=\rho a\sum_{m=-N}^{N-1}\int_0^\infty dt[u_m(t)]^2\ , \qquad (64)$$

which can also be obtained directly from the expression for θ, Eq. (56), by using the statistical independence of the numbers $u_{m_i}(t_i)$. With the Green function relevant for our simulations, Eq. (59), one obtains, for the variance,

$$\langle\theta^2\rangle=\sigma^2=(aG)^2\frac{\rho a^2 L}{4\pi^2\kappa_e}\sum_{k=-N}^{N-1}\frac{1-\cos(\pi k/N)}{k^2}\ , \qquad (65)$$

which for the parameters and units of Figs. 12(a) and 12(b) yields $\sigma=0.472\,80$ and $0.149\,51$, respectively, in four-figure agreement with the simulations. Although the expressions are more cumbersome, higher moments can similarly be checked.

We now ask the question: Does $P(\theta)$ have strictly exponential tails as suggested by the simulations and the mean-field theory of the preceding section? In order to answer this question we need to examine the analytic structure of $\hat{P}(q)$. To do this it is convenient to write

$$\ln\hat{P}(q)=-\rho\int_{-aG}^{aG}du\ W(u)(1-\cos qu)\ , \qquad (66)$$

where

$$W(u)=a\sum_{m=-N}^{N-1}\int_0^\infty dt\,\delta(u-u_m(t)) \qquad (67)$$

is the "density of states" of $u_m(t)$. In order to determine the analytic properties of (66), we need to obtain the analytic properties of $W(u)$. From the analytic expression for $u_m(t)$ it is clear that $W(u)$ has a singularity for $u=0$, which corresponds to large values of m and t. For a finite system, the asymptotic behavior of $W(u)$ eventually comes from large times only since m is then bounded by N. For large m and/or t, the asymptotic form of the Green function can be obtained from (59) by replacing the sum over reciprocal space by an integral to obtain the familiar continuum result

$$g_{0,m}(t)=aGH(t)\frac{a}{(4\pi\kappa_e t)^{1/2}}\exp\left[-\frac{m^2a^2}{4\kappa_e t}\right] . \tag{68}$$

For purposes of obtaining the asymptotic form of $W(u)$ for small u we may approximate $u_m(t)$ by

$$u_m(t)=-\partial_m g_{0,m}(t) , \tag{69}$$

when N is infinite. For N finite, on the other hand, the asymptotic behavior of $W(u)$ ultimately only comes from small m and large t. Expanding for large t, we obtain

$$u_m(t)=\frac{aG}{8\sqrt{\pi}}\left[\frac{a}{(\kappa_e t)^{1/2}}\right]^3(2m+1) , \tag{70}$$

where only $m=0$ and -1 contribute to the small-u limit of $W(u)$. The asymptotic form of $W(u)$ is now easily calculated by substituting Eqs. (69) and (70) into (67). For both finite and infinite N the asymptotic divergence of $W(u)$ is given by

$$W_\infty(u)=\frac{A_\alpha}{|u|^\alpha},\quad u\to 0 . \tag{71}$$

Interestingly, however, the exponent α and the corresponding amplitude A_α are different in the two cases. For N finite, we obtain $\alpha=\frac{5}{3}$ and

$$A_{5/3}=\frac{2}{3}\left[\frac{a}{(\kappa_e)^{1/2}}\right]^3\left[\frac{aG}{8\sqrt{\pi}}\right]^{2/3} . \tag{72}$$

For N infinite, $\alpha=\frac{5}{2}$ and

$$A_{5/2}=2\Gamma(\tfrac{5}{4})\left[\frac{2}{243}\right]^{1/4}\left[\frac{a}{(\kappa_e)^{1/2}}\right]^3\left[\frac{aG}{2\sqrt{\pi}}\right]^{3/2} . \tag{73}$$

When computing $W(u)$ numerically, a clean crossover from $\alpha=\frac{5}{2}$ to $\frac{5}{3}$ is observed when u becomes sufficiently small so that contours of constant u begin to run into the spatial boundaries of the space-time strip.

The analytic properties of $\hat{P}(q)$ are now clear: Since the integral

$$\int_0^{aG}du\,\frac{1-\cos qu}{u^\alpha} \tag{74}$$

is evidently an entire function in the q plane for α either $\frac{5}{2}$ or $\frac{5}{3}$, $\hat{P}(q)$ is entire in the q plane also. It follows that, for the simplified model under consideration, $P(\theta)$ cannot have strictly exponential tails. Even in one dimension, the long-range part of the Green function does not dominate and destroy the integrability of (74). We proceed via the saddle-point method to obtain the large-$|\theta|$ asymptotic behavior of $P(\theta)$.

The location of the saddle point satisfies

$$i\theta=\rho 2\int_0^{aG}du\;W(u)u\sin qu . \tag{75}$$

To keep the equations uncluttered, let θ be positive for now. The saddle point lies at $q=q_0=iy$, where y is real and large when θ is large. We scale out y to find

$$\theta=\frac{\rho}{y^2}2\int_0^{aGy}d\xi\;W(\xi/y)\xi\sinh\xi . \tag{76}$$

Because of the behavior of the small-u asymptotic form of $W(u)$, $W_\infty(u)$ [which, with $\alpha=\frac{5}{2}$, we find numerically to be a good approximation to $W(u)$ even when $|u|$ is of the order of aG], the integral (76) is dominated by its upper cutoff in the limit of large y. The asymptotic form of (76) is, therefore, given by

$$\theta=(aG)^2\rho W(aG)\frac{e^{aGy}}{aGy}\left[1-\left[1+aG\frac{W'(aG)}{W(aG)}\right]\frac{1}{aGy}+O\left[\frac{1}{(aGy)^2}\right]\right] , \tag{77}$$

or

$$\ln(\theta/\gamma)=aGy-\ln(aGy)-\left[1+aG\frac{W'(aG)}{W(aG)}\right]\frac{1}{aGy}+O\left[\frac{1}{(aGy)^2}\right] , \tag{78}$$

with $\gamma\equiv(aG)^2\rho W(aG)$. To get the leading behavior, we ignore the log and higher-order terms and just use

$$y=\frac{1}{aG}\ln(\theta/\gamma) . \tag{79}$$

Note that, within this approximation, γ is really only defined to within an arbitrary multiplicative constant of order unity. To leading order, $P(\theta)$ evaluated at the saddle point now becomes

$$P(\theta)=B\left[\frac{aG}{|\theta|}\right]^{1/2}\exp\left[-\frac{|\theta|}{aG}\ln|\theta/\gamma|\right] , \tag{80}$$

with $B=1/(aG\sqrt{2\pi})$, where we have generalized to θ having arbitrary sign. Thus, for large $|\theta|$, $P(\theta)$ becomes the PDF of a Poisson-like process.

The result (80) may be interpreted as follows: Given a volume Ω containing M identical objects, the probability p of finding n of them in a subvolume V is given by $\binom{M}{n}(V/\Omega)^n(1-V/\Omega)^{M-n}$. Taking Ω and M to infinity, keeping the density $\rho\equiv M/\Omega$ fixed, one obtains the Poisson distribution

$$P(n)=\frac{(\rho V)^n}{n!}e^{-\rho V}\simeq\frac{1}{\sqrt{2\pi n}}e^{-n\ln(n/e\rho V)-\rho V} . \tag{81}$$

If n flips are each to contribute an amount u so that $\theta\in(\theta,\theta+d\theta)$, then these flips must occur in a region of

space time where $u(t)\in(u,u+\delta u)$. The flips must, therefore, be found in a space-time volume $V=W(u)|\delta u|$. Since $n=|\theta/u|$, Eq. (81) gives the corresponding probability density $P(\theta)$ as

$$P(\theta)=\frac{1}{|u|\sqrt{2\pi}}\left[\left|\frac{u}{\theta}\right|\right]^{1/2} e^{-|\theta/u|\ln\{|\theta/u|/[e\rho W(u)|\delta u|]\}}, \tag{82}$$

where we have anticipated that only large n contribute to the asymptotics and have neglected the $\exp(-\rho V)\sim 1$ term. As we have seen in the preceding paragraph, all integrals were dominated by the upper cutoff $u=aG$, which means that in order to get a large value of θ, many flips must each contribute an amount u of order aG. Since $u\simeq aG$, the flips must have occurred for small t close to the point where the PDF is being observed, so that we may approximate $u=aG$ and $|u|e\rho W(u)|\delta u|=\gamma$ in Eq. (82). We thus recover the asymptotic form (80) from a consideration of elementary probabilities.

Figure 13 shows the tails of the numerical PDF of the simplified Kerstein model (54) and of the full Kerstein model (10) for the same parameters [see also Figs. 12(a) and 3(b) for the complete PDF's]. The asymptotic form (80), with B and γ as fitting parameters, fits both tails virtually perfectly with reasonable values for B and γ. The best fit to the noninterchanging flip simulation is obtained with $\gamma=0.0929=0.818(aG)^2\rho W(aG)$. In practice it is very difficult to distinguish $|x|\ln|x/(\text{const})|$ from $|x|$.

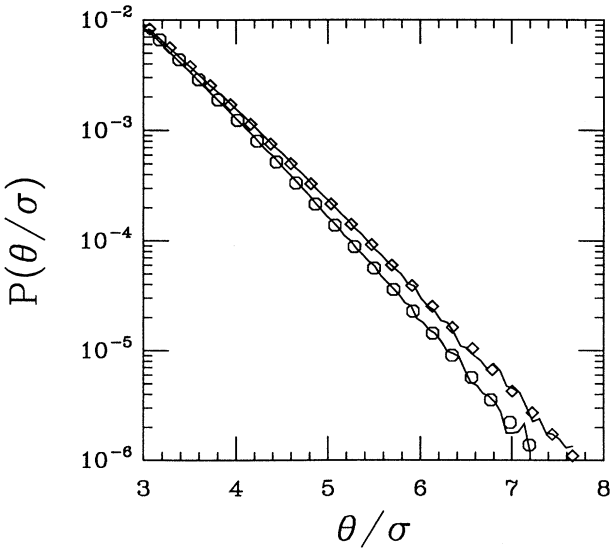

FIG. 13. Averaged data for the right tail of the PDF of Fig. 12(a) (noninterchanging Kerstein model, lower solid line) and of Fig. 3(b) (full Kerstein model, upper solid line). The octagons and diamonds indicate two-parameter fits of the form (80) with $(B,\gamma)=(1.108,0.09290)$ and $(B,\gamma)=(0.7169,0.1141)$, for the noninterchanging and full Kerstein models, respectively.

The fact that almost all of the tails of the numerical PDF's for the full Kerstein model show a slight downward curvature on a semilogarithmic plot lends some support to the presence of corrections to purely exponential tails. The exact, as yet unknown, asymptotic solution for the full Kerstein model is likely neither perfectly exponential nor $\exp[-|x|\ln|x/(\text{const})|]$, although clearly well approximated by either form. The same is even more likely to be true for any experimental data.

VI. SUMMARY AND CONCLUSIONS

We have studied the PDF of a turbulently advected passive scalar. Assuming the integral scale, or correlation length ξ_v to be much smaller than the system size, the scalar PDF probes the spatiotemporal organization of the flow on the integral scale and is insensitive to the details of the flow on smaller scales. We have, therefore, taken a mesoscopic point of view and coarse grained the system over a velocity correlation volume ξ_v^d. The action of an eddy of the velocity field on the scalar is modeled by an instantaneous "flip" followed by diffusion. The resulting model for the scalar was discretized on a lattice and is essentially equivalent to Kerstein's linear-eddy model [23]. We focused on the steady-state PDF of the scalar, in the presence of a linear mean scalar gradient, as a natural probe of the intrinsic effects of turbulent mixing.

The Kerstein model was implemented numerically in one and two dimensions with periodic boundary conditions and an imposed linear mean scalar gradient. The results were found to be insensitive to dimensionality and to the details of the implementation of the flip. For the physical range of parameters ($K\sim 1$), the PDF was found to have close-to-exponential tails. For rapid flip rates, $K\ll 1$, the PDF was closer to Gaussian, with a smooth change from Gaussian to exponential as K was increased to ~ 1.

The phenomenological mean-field-like theory of Ref. [18] was derived heuristically from the Kerstein model. This theory is formulated in terms of a nonlinear discrete mapping which treats the interplay between diffusion and advection in an, as yet formally unjustified, *ad hoc* way. Nevertheless, the theory appears to be in good qualitative agreement with our numerical results. For the case of a linear mean gradient, strictly exponential tails are predicted. The mean-field theory was also extended to the case of a finite system (δ-function boundary conditions) and to include effects of large-scale flow.

We also considered a simplified version of the Kerstein model. Under conditions of spatial homogeneity and imposed linear mean gradient, the mean-field theory for this model is identical to that of the full Kerstein model. For physically relevant parameters, the simplified model produces numerical PDF's virtually indistinguishable from those of the full Kerstein model. The asymptotic behavior of the PDF was shown to be of the form $\exp[-|\theta|\ln|\theta/(\text{const})|]$. The difference between this

asymptotic form and an exponential is subtle and our numerical data (and certainly all extant experimental data) cannot discriminate between the two forms.

Recent experimental results [20,19] suggest that the scalar fluctuations, in the presence of a linear mean gradient, are indeed close-to-exponentially distributed, lending some support to the approach taken here. At this point, the relevance of our models to the experiments of Libchaber and co-workers [8,9] is not clear.

ACKNOWLEDGMENTS

We thank Veit Elser, Jerry Gollub, Robert Kraichnan, Boris Shraiman, Eric Siggia, and Zellman Warhaft for helpful discussions. We are also indebted to Eric Siggia for a critical reading of the manuscript. We gratefully acknowledge support from the Cornell Materials Science Center (M.H.) and from the Air Force Office of Scientific Research, Grant Number 91-0011 (A.P.).

*Permanent address: Laboratoire de Physique Statistique, Ecole Normale Supérieure, F-75231 Paris, France. After January 1st, 1993: Institut Nonlinéaire de Nice, Parc Valrose, 06108 Nice CEDEX, France.

[1] A. Monin and A. Yaglom, *Statistical Fluid Dynamics* (MIT, Cambridge, MA, 1971).

[2] F. N. Frenkiel and P. S. Klebanoff, Phys. Fluids **8**, 2291 (1965).

[3] C. W. Van Atta and W. Y. Chen, J. Fluid Mech. **34**, 497 (1968).

[4] S. Tavoularis and S. Corrsin, J. Fluid Mech. **104**, 311 (1981) (in particular, see Figs. 21 and 22).

[5] C. W. Van Atta and W. Y. Chen, J. Fluid Mech. **44**, 145 (1970).

[6] Y. Gagne, E. Hopfinger, and U. Frisch, in *New Trends in Nonlinear Dynamics and Pattern Forming Phenomena: The Geometry of Nonequilibrium*, proceedings of a NATO Advanced Research Workshop, Cargèse, France, 1988, edited by P. Coullet and P. Huerre (Plenum, New York, 1990), p. 315.

[7] R. Antonia, E. Hopfinger, Y. Gagne, and F. Anselmet, Phys. Rev. A **30**, 2704 (1984); see also Y. Gagne, Thèse de Doctorat, Université de Grenoble, 1987.

[8] B. Castaing, G. Gunaratne, F. Heslot, L. Kadanoff, A. Libchaber, S. Thomae, X.-Z. Wu, S. Zaleski, and G. Zanetti, J. Fluid Mech. **204**, 1 (1989).

[9] M. Sano, X. Wu, and A. Libchaber, Phys. Rev. A **40**, 6421 (1989).

[10] K. Yamamoto and I. Hosokawa, J. Phys. Soc. Jpn. **57**, 1532 (1988); **58**, 20 (1989).

[11] M. Meneguzzi and A. Vincent, J. Fluid Mech. **225**, 1 (1991).

[12] R. Kraichnan, Phys. Rev. Lett. **65**, 575 (1990).

[13] Z.-S. She, Phys. Rev. Lett. **66**, 600 (1991).

[14] B. Castaing, Y. Gagne, and E. Hopfinger, Physica D **46**, 177 (1990).

[15] A. M. Oboukhov, Izv. Akad. Nauk SSSR, Ser. Geogr. Geofiz. **13**, 58 (1949).

[16] S. Corrsin, J. Appl. Phys. **22**, 469 (1951).

[17] R. Kraichnan, J. Fluid Mech. **64**, 737 (1974).

[18] A. Pumir, B. Shraiman, and E. Siggia, Phys. Rev. Lett. **66**, 2984 (1991).

[19] J. Gollub, J. Clarke, M. Gharib, B. Lane, and O. Mesquita, Phys. Rev. Lett. **67**, 3507 (1991).

[20] Jayesh and Z. Warhaft, Phys. Rev. Lett. **67**, 3503 (1991); Phys. Fluids A **4**, 2292 (1992).

[21] O. Métais and M. Lesieur, J. Fluid Mech. **239**, 157 (1992).

[22] S. T. Thoroddsen and C. W. Van Atta (unpublished).

[23] A. Kerstein, J. Fluid Mech. **231**, 361 (1991).

[24] If our model is to be applied to an experimental situation where the scalar fluctuates on scales much larger than ξ_v, then, at the very least, these fluctuations should be filtered out of the data before any comparison can be attempted.

[25] N. Weiss, Proc. R. Soc. London, Ser. A **293**, 310 (1966).

[26] H. Chen, S. Chen, and R. Kraichnan, Phys. Rev. Lett. **63**, 2657 (1989).

[27] V. Eswaran and S. B. Pope, Phys. Fluids **31**, 506 (1988).

[28] S. B. Pope, in *Studies in Turbulence: In recognition of contributions by John Lumley*, edited by T. Gatski, S. Sarkar, and C. Speziale (Springer-Verlag, Berlin, 1991).

[29] Y. Kimura and R. Kraichnan (private communication).

[30] The significantly less dramatic dependence of σ on K for the two-site flips [Figs. 3(a)–3(c)] is attributable to the strong discreteness in that case.

[31] The starting point in Ref. [18] was

$$\hat{P}_k(\mathbf{r},t+\tau)=-U(\mathbf{r},t)\cdot\nabla\hat{P}_k(\mathbf{r},t)+D\nabla^2\hat{P}_k(\mathbf{r},t)+\hat{P}^2_{k/2}(\mathbf{r},t)\ ,$$

which has also been studied in an engineering context by Nguyen and Pope [T. V. Nguyen and S. B. Pope, Combust. Sci. Technol. **42**, 13 (1984)]. Equation (26) is just the above equation without the $\mathbf{U}\cdot\nabla\hat{P}$ term representing the effect of advection due to large-scale velocity modes.

[32] See, e.g., G. F. Carrier, M. Krook, and C. E. Pearson, *Functions of a Complex Variable* (Hod, Ithaca, New York, 1983); see also U. Frisch and R. Morf, Phys. Rev. A **23**, 2673 (1981).

[33] P. Rhines and W. R. Young, J. Fluid Mech. **133**, 133 (1983).

[34] See, e.g., V. I. Arnold and A. Avez, *Ergodic Problems of Classical Mechanics* (Benjamin, New York, 1968), p. 8.

[35] Although any reasonable choice for Δ_n leads to the same physics, another natural choice is to take the Δ_n to be the lattice Laplacian, i.e.,

$$\Delta_n g_{n,m}=\frac{1}{a^2}(g_{n-1,m}+g_{n+1,m}-2g_{n,m})\ ,$$

which leads to the Green function

$$g_{n,m}(t)=\frac{aG}{2N}\sum_{j=-N}^{N-1}e^{i(n-m)ak_j}e^{2[\cos(ak_j)-1]\kappa_e t/a^2}H(t)\ .$$

This Green function has explicit periodicity in reciprocal space. Replacing the sum over reciprocal vectors by an integral, one obtains

$$g_{0,m}(t)=aGe^{-2\kappa_e t/a^2}I_m(2\kappa_e t/a^2)H(t)\ ,$$

where I_m is the modified Bessel function of the first kind of order m. All the results of Sec. V (except those which compare quantitatively with the simulations) can equally well be derived with this choice of Green function.

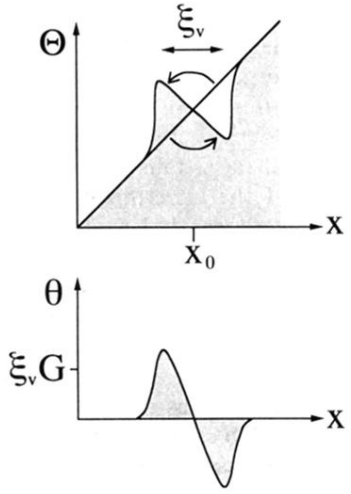

FIG. 1. The action of an eddy of size ξ_v centered at x_0 on the scalar field Θ as modeled by the Kerstein model. The eddy "flips" the scalar to the right of x_0 with the scalar to the left of x_0. When Θ has a mean gradient G, as shown, such a flip produces adjacent blobs of opposite sign and amplitude $\xi_v G$ in the fluctuations $\theta=\Theta-\langle\Theta\rangle$. These flips are performed instantaneously at a random set of space-time locations. Between flips, the scalar diffuses with an eddy diffusivity κ_e which tends to smooth the blobs out.